# Quantitative flow magnetic resonance angiography

## image analysis of iliac arteries in endurance athletes with sports related vascular problems

Penners, C.

*Award date:*
2005

TU/e technische universiteit eindhoven

máxima medisch centrum

# Quantitative Flow Magnetic Resonance Angiography:
Image analysis of iliac arteries in endurance athletes with sports related vascular problems

**Cindy Penners**

**June 2005**

**MRL/KFM 2005 – 01**

**Eindhoven University of Technology**
Faculty of Applied Physics

**Máxima Medical Center Veldhoven**
Department of Clinical Physics

**Supervisors:**
Dr. ir. C. van Pul
Prof. dr. ir. P.F.F. Wijn

## Voorwoord

Voor U ligt het resultaat van mijn afstudeerproject. Een jaar lang onderzoek op de afdeling klinische fysica van het Maxima Medisch Centrum Veldhoven in samenwerking met de afdelingen sportgeneeskunde en vaatchirurgie. Ik zou graag alle collega-studenten en medewerkers van de afdeling klinische fysica willen bedanken voor de gezellige werksfeer. Hoewel mijn uitgesproken Limburgse inbreng niet altijd op prijs werd gesteld heeft het tot heel wat interessante conversaties geleid. Ik zou in het bijzonder willen bedanken, Professor Pieter Wijn, voor de opbouwende kritiek, inspiratie en interessante discussies. Carola van Pul, hoewel je er niet altijd kon zijn door je promotie en Zuid-Amerika reis heb je me geweldig begeleid, geholpen en geleerd hoe het is om een echte fysicus te zijn. Vaatchirurg Mart Bender en sportarts Goof Schep wil ik bedanken voor hun inbreng in het project vanuit de kliniek. Ook zou ik Gijs Klerkx willen memoreren. Hij heeft me gedurende de eerste maanden van mijn afstuderen met zijn enthousiasme, geduld en eeuwige vrolijkheid ontzettend geholpen om de vraagstelling en achterliggende problematiek bij duursporters te begrijpen. Helaas is hij op veel te jonge leeftijd van ons heengegaan.
Tevens is dit verslag het eindproduct van mijn studie Technische Natuurkunde. De weg hiernaartoe is niet altijd even makkelijk geweest en ik heb heel wat tegenslagen moeten overwinnen, maar gelukkig niet alleen. Daarvoor een woord van dank aan mijn ouders, die ondanks hun eigen moeilijke situatie me altijd zijn blijven steunen. En een woord van dank aan alle familie en vrienden die altijd in me zijn blijven geloven.

Cindy Penners

Sittard, 29-05-2005

## Abstract

Endurance athletes, like cyclists can suffer from vascular problems (e.g. stenosis) in the iliac arteries, due to extreme hip flexion and hypertrophy of the psoas muscle. The purpose of this research was to retrospectively analyse MR examinations of endurance athletes to determine differences (both anatomical and functional) between healthy and affected arteries.

The patient group consisted of endurance athletes suffering from severe vascular problems in the left external iliac artery. Reference values were obtained from a control group (endurance athletes with healthy arteries) and healthy volunteers (no history of endurance sports). The MR exams included Phase Contrast Angiography (PCA) to obtain quantitative flow (QF) information. Various segmentation techniques were developed and tested to semi-automatically detect the arteries in the MR images, e.g. a threshold, and active shape technique. Following segmentation the velocity information in the arteries of interest was extracted and the diameter and cross sectional area of the arteries were calculated.

The comparison of different segmentation techniques led to the choice of active shape segmentation as the preferred method for vessel detection. As most patients suffered from vascular problems in only one leg, a comparison could be made between the left and the right leg. The patient group showed a clear difference between the stenosed and the healthy external iliac artery: In the first the cross sectional area of the vessel was smaller and the peak systolic velocity increased to compensate for the flow. Due to large inter-human variability in the evaluated parameters no comparison could be made between patients and controls. A volunteer study showed a substantial difference in the parameters between different heart beats. Furthermore the error introduced by misalignment in the planning was of the same order as the variability between heartbeats.

In conclusion, even slightly stenosed arteries display a reduced cross sectional area and increased velocity when compared to the healthy artery in the other leg of the same patient. However, large variation in the evaluated parameters between left and right leg in controls and at non-affected regions of patients was observed, which makes the described method of PCA imaging and analysis unsuitable for individual diagnosis. From the volunteer study we can conclude that the current method of acquiring the PCA images is reliable.

In further research we have to make the step from 2D PCA to 3D PCA and use the quantitative flow information in the whole stenosed part of the artery instead of in one slice. This will give more information concerning the seriousness of the vascular problem.

# Table of contents

# 1 Sports-related flow limitations in the iliac arteries in endurance athletes

Vascular problems in endurance athletes were first described in 1986 by Chevalier et al. [1]. They described a new disease, endofibrosis, an injury of the inner vessel wall. Endofibrosis mainly occurs in well-trained cyclists. The patients have very typical *claudication*[1]-like complaints in the legs at maximum effort, like a powerless feeling or cramp. As a result of these complaints, they have to stop their sports activities. At rest the complaints disappear quickly within 1 to 4 minutes. The complaints predominantly occur in the left leg. Even in today's (sports) medical practice the diagnosis is often missed, because a vascular problem is not expected in healthy athletes [1-3].
In this chapter a brief review will be given of these vascular problems in athletes. First the anatomy of the vessels, muscles and joints in the leg is described. Then a closer look at the aetiology causes will be presented together with an overview of the methods currently used for diagnosis. Finally the purpose and outline of this graduation thesis will be discussed.

## 1.1 Anatomy

The aorta originates from the left ventricle of the heart; via the arch of aorta it bends *ventral* to the *spinal column* in the direction of the *coccyx*. At the level of the fourth *lumbar vertebra* it bifurcates in the right and left common iliac artery. In the pelvis both arteries bifurcate again in the external and internal iliac arteries. The internal iliac artery transports blood predominantly to the muscles in the pelvis area, like the psoas muscle. Finally the external iliac artery becomes the femoral artery and provides the lower leg with blood. An overview of these vessels and the bifurcations in the leg is shown in Figure 1.1 [4].

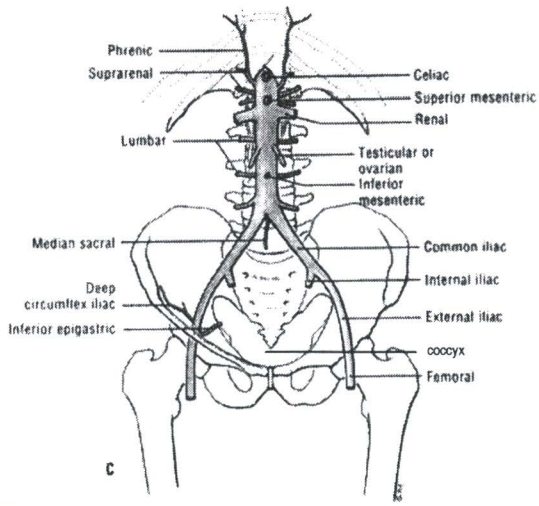

*Figure 1.1: Overview of the vessels and bifurcations [4]*

The iliac arteries are lying ventral to the hip joint, passing over the psoas muscle. During flexion of the hip the arteries have to shorten (Figure 1.2 a and b). Most of this shortening can be accomplished by the natural elasticity and smooth bending of the arteries. However, a pathological fixation of the arteries to tissues, e.g. the psoas muscle, can strongly limit the possibility of shortening, resulting in bending or even kinking of the arteries [5]. Kinking can also occur during extreme flexion (Figure 1.2 c) of the hips (aerodynamic position on the bicycle), or due to *hypertrophy* of the psoas muscle, which forces the artery in a more ventral position (Figure 1.2 d). A combination of the causes for kinking, as described above, enlarges the risk of kinking.
Natural fixations of the iliac arteries are the aorta bifurcation and the branching of the femoral artery in the *groin*. The bifurcation of the common iliac artery is mobile under normal conditions. During hip flexion the common iliac artery and the external iliac artery together accomplish the shortening.

[1] All Italic printed words in the text are translated and explained in the terminology list (appendix 1)

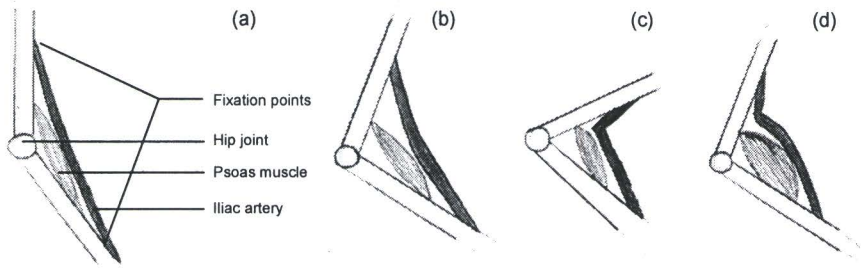


*Figure 1.2: Schematic drawings of the hip: (a) stretched, (b) during flexion , (c) extreme flexion and (d) hypertrophy of the psoas muscle.*

## 1.2 Aetiology

In athletes with flow limitations in the iliac artery, *adhesions* were observed at the bifurcation of the common iliac artery. In addition, fixations of the external iliac artery to the psoas muscle were observed [5]. These fixations disturb the natural process of bending and shortening of the arteries. If the artery cannot accommodate the excessive length anymore, this may result in kinking.

Due to kinking the diameter of the vessel decreases. This results in an increase of flow to maintain the same blood supply to the vessels. Also the flow pattern will become more irregular and the hemodynamic load on the vessel wall will increase. This can result in damage to the intimal (Figure 1.3) of the vessel resulting in endofibrosis, which is defined as a thickening of the intimal of a vessel consisting of collagen, fibroblasts and smooth muscle cells. The medial and adventitial remain healthy [5]. In 90% of the patients (athletes with vascular problems), endofibrosis is found in the external iliac artery, in 5% in the common iliac artery and in 10% in the femoral artery [5].

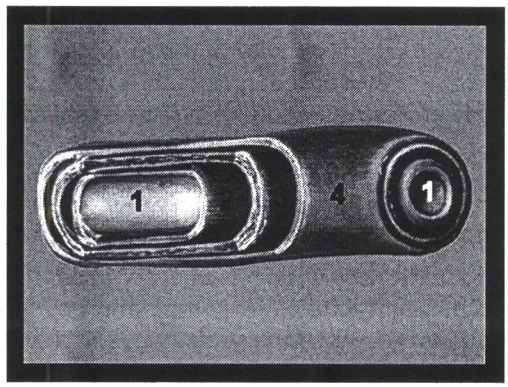


*Figure 1.3: Schematic representation of an artery, with 1 the lumen, 2 intimal, 3 medial and 4 adventitial.*

In literature two explanations are given for the complaints of the athletes. Both explanations pose that the complaints are caused by the limitation of the blood flow as a result of a *stenosis*. However, the cause of the stenosis is still subject of discussion. Chevalier states that the stenosis is caused by endofibrosis [1], while Schep showed that the stenosis could be caused by kinking, without intravascular damage [2, 3, and 5].

## 1.3 Sports related vascular problems in the iliac arteries

The flow limitations in endurance athletes are related to their sports activities. Especially cycling and skating are endurance sports characterised by a large demand of blood in the legs, combined with intermittent hip flexion. Professional cyclists will cycle approximately 35,000 km a year corresponding with 8,000,000 hip flexions [5]. During exercise the demand for blood from the muscle increases. At maximum effort flow through the iliac arteries can reach up to 10 litres per minute resulting in a huge increase of the hemodynamic load on the vessels [2, 3, and 5].

The cycling position is also an important factor in the development of vascular problems in the iliac arteries. Competition cyclists are always searching for the most

aerodynamic position. This is accomplished by keeping the back as horizontal as possible, resulting in an increase of hip flexion. With increasing hip flexion the vessel has to achieve an excessive shortening, to fit in a smaller space. This can result in kinking.
With the introduction of the click pedal it became possible to combine a push (down) phase of a cycle with a pull (up) phase. In general, it is assumed that this leads to an increase of speed [5]. The pulling is done by hip flexors, of which the psoas muscle is the most important. This can result in hypertrophy of the psoas and an increase of the chance of kinking. From research of Coyle et al. [6] it was concluded that most professional cyclist don't use the pull phase, to gain more power in the push phase. So the pull phase is apparently not really necessary, but can be harmful by the increased risk of kinking.

## 1.4 Currently used methods

At the moment several tests are performed on cyclists with the complaints described in the previous section. An examination starts with the evaluation of the patient's history and a short physical examination. Then a series of quantitative measurements start consisting of blood pressure measurements during exercise, Echo-Doppler (ultrasound) and magnetic resonance angiography (MRA). By combining the results of these tests a diagnosis can be made. This section will briefly discuss these tests, together with several new methods, which are still in the research stadium. MRA will be explained in more detail in chapter 3.

### 1.4.1 Patient history

Every examination of a new patient starts with an investigation of the patient's history. The patient is asked to fill in a questionnaire on basis of which the physician in sports medicine has a conversation with the patient. The main goal is to find out where and when the complaints occur. It is also important to exclude patients with problems other than vascular problems but with similar complaints like overtiredness or neurological pains.

### 1.4.2 Physical examination

During the physical examination, the physician listens to the groin artery with a stethoscope. This is done at two positions of the patients; with stretched leg and flexed hip. An irregular noise in the sound of the blood flow might be an indication of a stenosis. Furthermore the physician tries to get an impression of the symmetry of the hip joints during simple movements, like hip flexion and bending sideward.

### 1.4.3 Blood pressure during exercise

When the blood flow *distal* to a stenosis is insufficient, the local blood pressure will decrease. By comparing of the blood pressures close to the heart (arm) and after the presumed stenosis (ankle), the presence of a stenosis can be detected. In rest, the stenosis has to occupy at least 75% of the artery before a difference in blood pressure can be measured [7]. For small stenosis this method seems unsuitable. To solve this problem, blood pressure measurements are done after maximum exercise. During exercise the smaller arteries in the muscles expand. These expanded vessels can deliver more blood to the muscles than can be supplied by the stenotic artery. The amount of blood in the artery distal to the stenosis decreases fast, resulting in a drop in blood pressure.
Non-invasive measurement of blood pressure during heavy exercise is difficult. At the moment these measurements are performed directly after the exercise. The blood pressure measured in the ankle divided by the blood pressure in the arm is denoted as the ankle-arm index. Chevalier et al. [8] considers an ankle-arm index of less than 0.5 as an indicator for a vascular problem. Ankle-arm indices between 0.5 and 0.7

are in the marginal area. Most of the patients with this index value were diagnosed later to have a vascular problem [9]. Currently Schep [7] uses an ankle-arm index of 0.54 as a criterion for vascular problems. When a patient has *unilateral* complaints, comparison of the ankle-arm index on both sides has proved to be a very reliable indicator for a stenosis on the side of the complaints.
Disadvantage of this method is the time delay between the maximum exercise and the actual measurement. Due to this time delay, the stenosis can be missed in the diagnosis.

### 1.4.4 Echo-Doppler examination

With Echo-Doppler the arteries can be visualised and blood flow velocities can be calculated. The blood flow velocity can be used as an indicator for stenosis. Due to a stenosis the vessel diameter becomes smaller, which leads to an in increase in velocity. For stenosis occupying up to 20% of the lumen of a vessel, only small changes can be seen. However for stenosis occupying between 20% and 49% of the lumen, an increase of 30 to 100% of the peak systolic blood velocity (PSV) is observed, compared to a healthy artery [7]. Furthermore, ultrasound examinations can visualise a thickening of the vessel wall or kinking due to an excessive length. Ultrasound images of the external iliac artery in a healthy volunteer, an intravascular *lesion* and kinking are shown in Figure 1.4 a, b and c respectively.

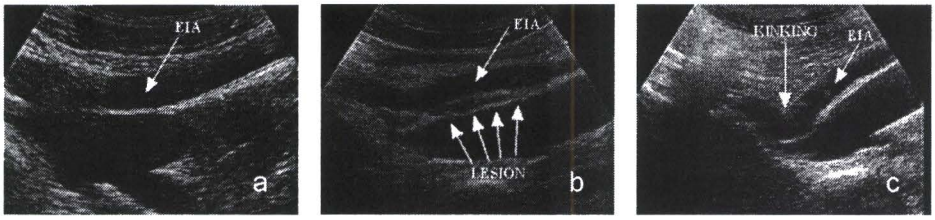


*Figure 1.4 Examples of images made with ultrasound from (a) a healthy artery, (b) an artery with a stenotic lesion and (c) an artery with severe kinking. EIA is external iliac artery [5].*

### 1.4.5 MRA

Magnetic Resonance Imaging (MRI) is an imaging technique capable of imaging soft tissues of the body. The technique will be discussed in detail in chapter 3. Magnetic resonance angiography (MRA) is a MRI technique used to visualise the blood vessels. Its main advantage is that the blood vessels can be viewed in three dimensions from every angle. Various MRA techniques, used for the examination of cyclists and other endurance athletes with symptoms suggesting vascular problems, are also described in chapter 3. The most important MRA technique for this research is the phase contrast MRA. This provides both anatomical and quantitative flow (QF) information from the blood vessels.

### 1.4.6 New methods

Several new methods are currently investigated on their usefulness for diagnosing vascular problems in endurance athletes. Two examples are pedal force measurements and $O_2$ consumption in the muscles, with near infrared spectroscopy (NIRS). Both methods are still in development and will not be further discussed.

## 1.5 Purpose

The purpose of this research was to retrospectively analyse the MR examinations of endurance athletes by using quantitative flow (QF) information. The main research questions were:

- Can significant differences be detected in the QF images between the vessel in the leg with a stenosis and the healthy leg? Parameters of interest are the change in diameter, cross sectional area, maximum velocity and flow during the heart phase.
- Can the wall shear stress be determined from the velocity information of the QF images and is there a difference between the healthy leg and the one with a stenosis?

For a better understanding of the flow pattern in vessels with kinking or other flow limitations, a review on vascular mechanics will be given in chapter 2. With a flow model predictions can be made about the hemodynamic load on the vessel wall.
Basic principles of MRI and the method for acquiring QF images are described in chapter 3. To be able to answer the questions in this research, the velocity information has to be extracted from the QF images and an accurate image segmentation technique is needed. This image segmentation is a complex process that can be performed in several different ways. In chapter 4, the various algorithms and the implementation of two of them will be discussed.
Finally it is important to optimize the protocol used for MRI-scans. The advantages and disadvantages of different methods will be tested in a volunteer study. Chapter 5 will discuss the results of both the retrospective and the volunteer study.

# 2. Cardiovascular Fluid Mechanics

Cardiovascular fluid mechanics (CFM) is a collective term for all mechanics involved in the vascular system. Because of the pulsatile flow, the branching and elasticity of the walls CFM is a very complex subject. This chapter will only deal with the basic concepts and the parameters of interest for the present research. More detailed information on the subject can be found in textbooks and lecture notes [10, 11].

## 2.1 Flow in arteries

In this section a brief overview will be given on the theory of flow in arteries. Most endurance athletes have elongated, and therefore bended, vessels. After a brief introduction on general fluid mechanics, the flow profile in curvatures is discussed. In this research we are primarily interested in the external iliac artery closely beyond the iliac bifurcation. For this reason we will also discuss the expected flow profile distal to a bifurcation. Furthermore the influence of the pulsatile nature of the flow on the velocity profile will be discussed.

### 2.1.1 General fluid mechanical considerations

For understanding the flow in curvatures and bifurcations, as present in the human circulatory system, some understanding of the basic principles of fluid mechanics is needed.

The fundamental principles of fluid mechanics are the conservation of mass and momentum. In most fluid mechanical problems it is convenient to define parameters that scale with the volume; mass and force are replaced by density ($\rho$, mass per volume) and stress (force per unit area). Stresses can be further classified as pressure (P, normal stress) and shear stresses ($\tau$, tangential stresses).

Fluids can be classified by their behaviour under stresses. Fluids with constant viscosity, not dependent of the rate of shear, are called Newtonian fluids. Although blood is generally not Newtonian due to its constituents, in large vessel hemodynamics it can be approximated as such, because of the negligible length scale of the blood cells with respect to the characteristic length of the arterial dimensions and the relatively high shear rates. Another important assumption in defining blood as Newtonian is the "no-slip condition", a fluid in contact with a solid does not move relative to the solid. Until now there are no reasons to doubt the applicability of this assumption to the arterial lining of endothelial cells [12].

A very important parameter in characterizing the flow is the Reynolds number ($Re$), which can be thought of as the dimensionless ratio of the inertial forces (order: $\rho v^2$) and viscous forces (order: $\mu v/d$):

$$Re = \frac{\rho \cdot v_{char} \cdot d}{\mu}, \tag{2.1}$$

with $\rho$ the density of blood ($\approx 1 \cdot 10^3$ kg/m$^3$), $v_{char}$ the characteristic velocity, $d$ the characteristic length and $\mu$ the dynamic viscosity of blood ($\approx 4 \cdot 10^{-3}$ N·s/m$^2$). When $Re$ is very small, the viscous forces dominate the flow. At very large $Re$ the flow acts inviscid, except for boundary layers near walls. $Re$ in the human circulation varies between $5 \cdot 10^3$ in large arteries, and $1 \cdot 10^{-2}$ in small arterioles [12].

Considering flow in a straight rigid tube, there is a phenomenon called entry flow. Starting with a uniform flow at the entrance it develops, due to the no-slip condition, to the familiar Poiseuille profile (Figure 2.1).

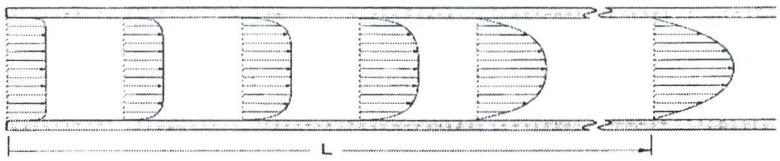


*Figure 2.1: Development of Poiseuille profile, L= entrance [12]*

The entrance length $L$, needed to establish fully developed flow, depends on $Re$ (with $v_{char}$= mean velocity and $d$ = the diameter of the tube):

$$\frac{L}{d} \approx 0.03 \cdot \mathrm{Re} \rightarrow L \approx 0.03 \cdot \frac{\rho \cdot v_{char} \cdot d^2}{\mu}, \tag{2.2}$$

In the large arteries no fully developed flow will be seen, e.g. in the aorta a length of approximately 3 m would be necessary to let the flow develop. Therefore in most arteries no Poiseuille profile occurs, but a plug flow as shown on the left of Figure 2.1.

We take the same rigid tube with a restriction in diameter now. Converging cross sectional area combined with the conservation of mass requires an increase of the average velocity (Figure 2.2) resulting in narrowing of the boundary layer. In the diverging part, after the restriction, the opposite happens; the flow decelerates and the boundary layer thickens. This is the change in pattern that could be observed in vessels with a stenosis or thickening of the intima (Section 1.2).

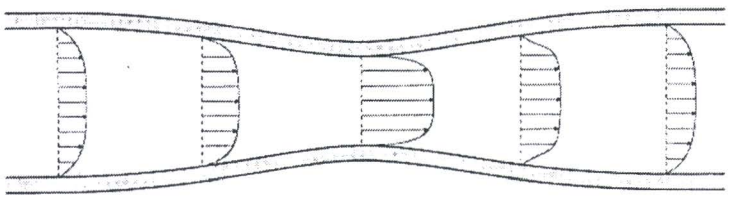

*Figure 2.2: Steady flow in a converging/diverging tube. The fluid accelerates in the converging part (1-3) and decelerates in the diverging section (3-5). [12*

### 2.1.2 Flow in curvatures and bifurcations

If we consider steady flow in a curved tube, the flow will depend on an other dimensionless parameter, the Dean number ($De$):

$$De = \sqrt{\frac{a}{R}} \cdot Re, \tag{2.3}$$

with $a$ the radius of the tube and $R$ the radius of curvature. The Dean number is a measure for the turbulence in a curved tube and can also be related to the wall shear stress [13]. The original form of the Dean number was formulated for tubes of constant cross section and for fully developed steady flow. Neither of these conditions applies to the human circulatory system and therefore we can only use it here as a rough indication of the turbulence in arteries. $De$ varies from nearly zero in relative straight arteries to the order of hundreds in more highly curved arteries (e.g. the aortic arch).

Centrifugal forces play an important role in the development of a complicated velocity profile. Centrifugal force per unit of volume is defined as:

$$F_c = \frac{\rho \cdot v^2}{r}, \tag{2.4}$$

with $\rho$ the density of the circular moving particle, $v$ the velocity and $r$ de radius of curvature. This force is greatest in the axial streams, because the fluid there is moving fastest and least near the walls, where the liquid is moving slow due to viscous forces. The centrifugal force creates a change in pressure (pressure

gradient) along the cross section of the tube, with the highest pressure on the outside curve. In the boundary layer the force caused by the pressure gradient is not in equilibrium with the centrifugal force. This results in a net force along the wall from the outside to the inside curve (secondary flow). Conservation of mass demands a compensative flow in the core of the tube. Two secondary flows are set up within the tube separated by the medial plane in the line of the radius of curvature. This is shown in Figure 2.3; the side-view shows the displacement of the axial flow to the outer wall. Secondary flows are shown in the cross section (upper left) of Figure 2.3 [14], with arrows denoting de direction of the flow.

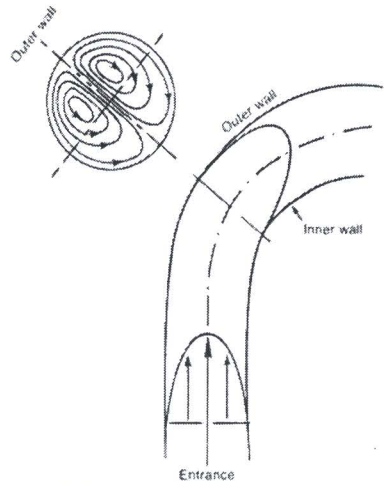


*Figure 2.3: Velocity profile in a curvature [14]. The side view shows the displacement of the axial flow and the cross section (upper left) shows the secondary flows.*

Besides curvatures, branching occurs in the vascular tree. The fluid mechanical description of a bifurcation is very complex, even if we consider a symmetric bifurcation. Even for a simplified description much additional information is needed like branching angle, sharpness of flow divider (Figure 2.4) and geometry in the neighbourhood of the bifurcation. It is not difficult to construct a qualitative picture of the expected flow profile after the bifurcation. If we start with a Poiseuille profile in the parent tube, the flow is split in two streams by the flow divider. A new boundary layer is formed in both daughter tubes on the inside wall of the bifurcation, with maximum axial velocity just outside this boundary layer. Since both daughter tubes can be seen as branching off in a curvature, secondary flow profiles arise again. These flow phenomena in a bifurcation are all schematically drawn in Figure 2.4.
More detailed information of flow in bifurcations can be found in a variety of articles, e.g. [15, 16].

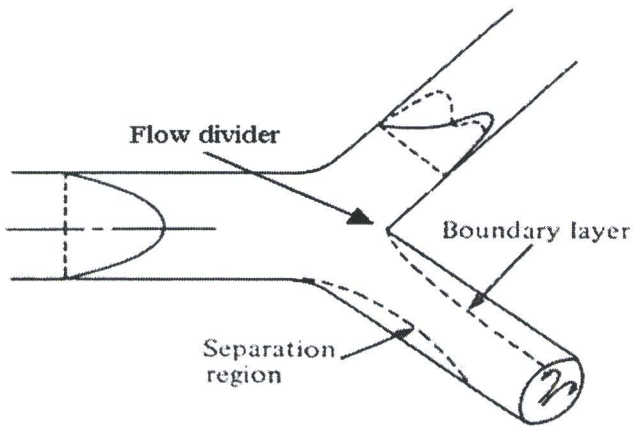


*Figure 2.4: Qualitative picture of flow downstream a single bifurcation, with Poiseuille flow in the parent tube. Direction of secondary motions, new boundary layer and separation region are indicated in the lower branch. In the upper branch the velocity profile in the plane of the bifurcation (continuous curve) and the normal plane (broken curve) are indicated. [17]*

### 2.1.3 Pulsatile flow

Pulsatile or oscillatory flow, like in the human circulatory system caused by the heart beating, makes the velocity profiles and governing equations much more complicated. Womersley [18] laid the foundation of a linearized model for the analysis of pulsatile flow in straight tubes. He assumed that motion was limited to the axial direction. These assumptions finally lead to an expression for the velocity profile in axial direction. An important parameter in his theory is the Womersley number, $\alpha$, defined by:

$$\alpha = a \cdot \sqrt{\frac{\rho \cdot \omega}{\mu}}, \tag{2.5}$$

with $a$ the radius of the tube and $\omega$ the frequency of the pulsatile flow. When $\alpha$ is small the flow can be considered quasi-steady. At large $\alpha$, the viscous effects are confined to the region near the tube's wall (Figure 2.5). In the circulatory system $\alpha$ varies from the order of 10 in large arteries to the order of $10^{-3}$ in arterioles. The Womersley number is a very important parameter in analyzing unsteady flows and is proportional to the ratio of the radius of the tube and the thickness of the boundary layer near the tube's wall ($\delta$). The boundary layer thickness is defined as:

$$\delta = \sqrt{\frac{\mu}{\rho \cdot \omega}} \tag{2.8}$$

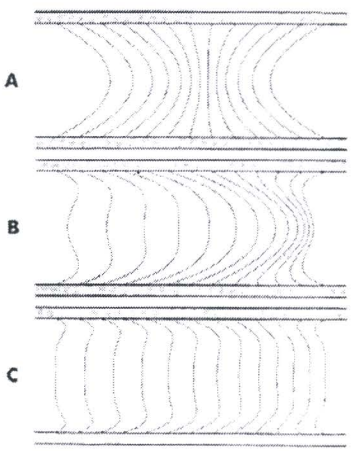


Oscillatory flow in a curved tube is more difficult to describe, since the velocity is no longer in the direction of the pressure gradient caused by the heart beating. This introduces nonlinear terms in the equation and only several particular cases can be solved [19].

*Figure 2.5: Womersley flow for a sinusoidal pressure gradient in a straight tube of circular cross section. The different curves represent the velocity profiles at different times and are displaced for clarity. The zero for each curve is given by the points at the wall. The flow is shown for only half of the cycle.* **A**→$\alpha$=1, **B**→$\alpha$=4, **C**→$\alpha$=8.

### 2.1.4 Predictions for the iliac arteries

In most people the iliac arteries are relatively straight, e.g. see Figure 2.6. In these vessels the approximation of a straight tube can be used. After the bifurcations (aorta and iliac bifurcation) flow profiles, as sketched in Figure 2.4, are expected. Figure 2.7 shows a profile as measured in the same volunteer as shown in Figure 2.6. The slice was chosen perpendicular to the right external iliac artery approximately 2 cm below the iliac bifurcation. The expected asymmetric velocity profile is recognisable in this figure.

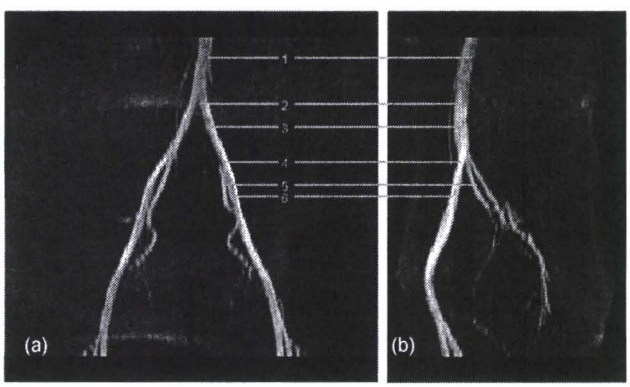


*Figure 2.6: MRI images of blood vessels in a healthy volunteer. Front view (a) and side view (b). Indicated are: 1) Aorta, 2) Aorta bifurcation, 3) Common iliac, 4) Iliac bifurcation, 5) Internal iliac and 6) External iliac*

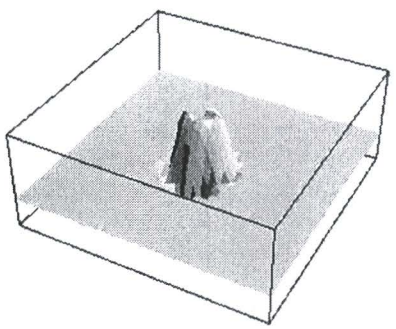

*Figure 2.7: Velocity profile as measured in the same volunteer as Figure 2.6.*

An example of a cyclist with extended vessels is shown in Figure 2.8. These vessels show more curvatures, even in stretched position. This increases the risk of kinking in endurance athletes. The many curvatures also cause complex flow profiles and even some turbulence, due to high Dean numbers. Secondary flows and vortices will occur. A velocity profile as shown in Figure 2.7 is difficult to make for these vessels, because they appear very spiky as a result of the complex flow and turbulence. With the MR method used in this study the velocity is only measured perpendicular to the chosen slice and velocity in other directions can not be visualised. Using the simplified equations presented in the previous sections is no longer allowed here and predicting the flow has become more complex. It requires meshing, *CFD* package, large computers etc. An overview of the current possibilities in this field can be found in [20].

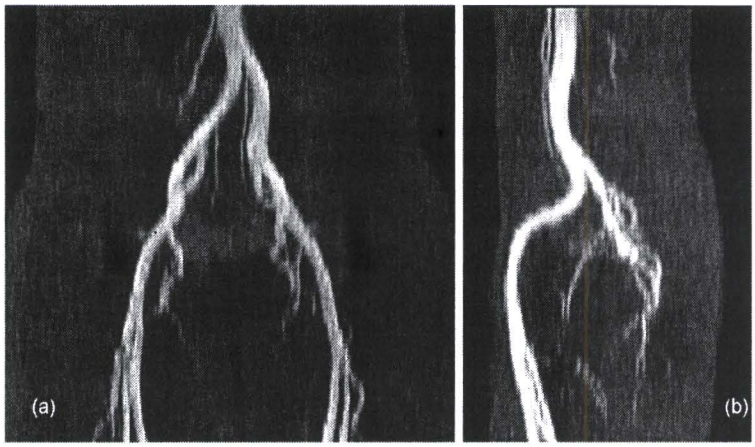


*Figure 2.8 Example of extended and curved blood vessels in an endurance athlete. Front view (a) and side view (b).*

## 2.2 Wall shear stress

The formation of endofibrosis (section 1.2) is thought to be closely related to the physical forces acting on the interface between the flowing blood and the arterial wall. The main hemodynamic factor is probably the wall shear stress. Wall shear stress is the term for mechanical stresses on the vessel wall exerted by the flowing blood [21].

$$\tau = \mu \left. \frac{\partial u}{\partial r} \right|_{wall}, \tag{2.9}$$

with $\tau$ the wall shear stress (WSS), $\mu$ the dynamic viscosity and $\partial u/\partial r$ the shear rate (change in velocity unit per change in radial distance unit). The correlation between WSS and atherosclerosis has been investigated [22] and it has been reported that atherosclerosis is likely to develop in regions with low or oscillating WSS. Although endofibrosis does not resemble atherosclerosis in composition and initiation factors it is thought to develop under similar stress conditions [5].

### 2.2.1 Effect of wall shear stress on the endothelial cells

In a study on atherosclerosis it has been shown that WSS can change the morphology and orientation of the endothelial cell layer [22]. Endothelial cells subjected to elevated levels of WSS tend to elongate and align in the direction of flow, whereas those experiencing low or oscillatory WSS remain more rounded and have no preferred alignment pattern. Furthermore, the levels of vasoactive substances released by endothelial cells are strongly influenced by wall shear stress. Non-pulsatile high wall shear stress promotes the release of factors from endothelial cells that inhibit coagulation, migration of leukocytes and smooth muscle proliferation,

while simultaneously promoting endothelial survival [22]. These are probably the basic principles of endofibrosis formation.

### 2.2.2 Determination of the wall shear stress

Quantitative flow (QF) images made with the PCA (an MRI technique described in section 3.2.1) technique make it possible to measure WSS in vivo, *non-invasively*. A method for determination of WSS, within PCA images is described by Oyre et al. [21]. The accuracy of this method depends on the accuracy with which the velocity profile can be measured at the vessel wall and the exactness of determining the position of the vessel wall within a pixel (sub-pixel edge detection, Figure 2.9 a).

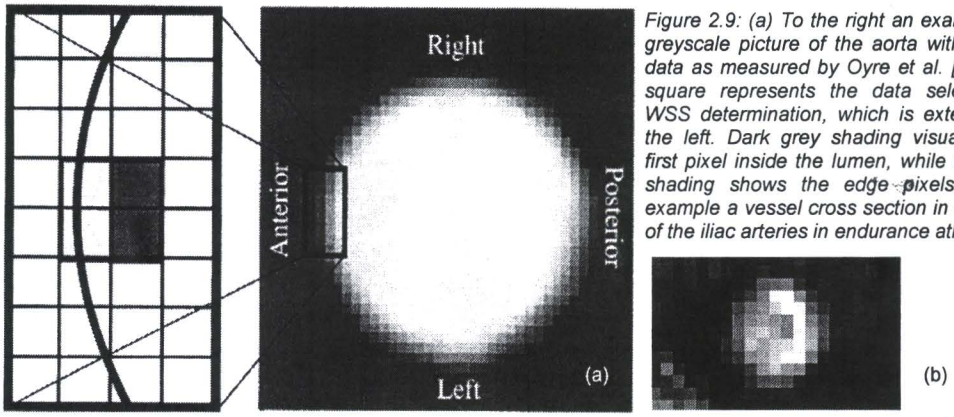


*Figure 2.9: (a) To the right an example of a greyscale picture of the aorta with velocity data as measured by Oyre et al. [21].. The square represents the data selected for WSS determination, which is extended tot the left. Dark grey shading visualizes the first pixel inside the lumen, while light grey shading shows the edge pixels. (b) An example a vessel cross section in our study of the iliac arteries in endurance athletes.*

The application of this method by Oyre is only possible when high resolution PCA images are available. Oyre et al. used PCA images of the aorta, with a pixel size of 0.25 $mm^2$. The images of endurance athletes available for this project have a pixel size of 1 $mm^2$ and the vessels are relatively small compared to the aorta (Figure 2.9 b). Further optimization of the imaging sequence to image on a higher resolution was not possible since the SNR was too low and taking more averages not possible in the available scan time. Furthermore a very accurate detection of the blood vessel in the MR images is needed. As will be described in chapter 4, this is still difficult. Applying this method on the images in this project would give very inaccurate results.

## 2.3 Arterial stiffness

Another parameter of interest for this research is the local arterial stiffness, which is a dynamic property based on vascular function and structure and depends on arterial pressure [23]. Two important indices of arterial stiffness are arterial *distensibility* (D) and arterial *compliance* (C), both expressed with their corresponding coefficient. The compliance coefficient (CC) is defined as the change in cross-sectional area ($\Delta A$) per unit of pressure ($\Delta P$) and can be calculated as follows [23]:

$$CC = \frac{\Delta A}{\Delta P} = \frac{\pi\left(2d \cdot \Delta d + \Delta d^2\right)}{4\Delta P}, \tag{2.14}$$

with $d$ the diameter and $\Delta d$, the change of diameter during the heart cycle (distension). Likewise the distensibility coefficient (DC) is defined as the relative change in cross-sectional area ($\Delta A/A$) per unit of pressure ($\Delta P$).

$$DC = \frac{\left(\Delta A / A\right)}{\Delta P} = \frac{\left(2\Delta d \cdot d + \Delta d^2\right)}{\left(\Delta P \cdot d^2\right)}, \tag{2.15}$$

ΔP during the heart cycle is equal to the Pulse Pressure (PP) and calculated as systolic blood pressure (SBP) minus diastolic blood pressure (DBP). Diameter and change in diameter can be determined reasonably reliable from MR images and will be described in chapter 4. A major source of error using this method may be the accurate assessment of the local PP. The PP should be measured at the site of the distension measurements and preferably non-invasive. In most parts of the human body this is very difficult. Various methods for PP assessment and determining the arterial stiffness are discussed by Bortel et al. [23].

# 3 Imaging techniques

This chapter will start with a brief introduction into MRI. Then various angiography techniques will be discussed in more detail. For detailed information about MRI the reader is referred to textbooks [24 – 26].

## 3.1 Magnetic Resonance Imaging

A nucleus abundant in the human body is the hydrogen nucleus (a single, positively charged proton). This spinning charged particle possesses a magnetic moment. If protons are placed in an external magnetic field, they will line up with that magnetic field, either parallel or anti-parallel, resulting in a net magnetization parallel to the external magnetic field. The magnetic moment of the proton will precess around the direction of the external magnetic field (figure 3.1), defined in z-direction. The rotation frequency is given by

$$\omega_0 = \gamma \cdot B_0, \tag{3.1}$$

with $\omega_0$ the Larmor frequency, $B_0$ the strength of the external magnetic field and $\gamma$ the gyromagnetic ratio ($\gamma / 2\pi$ = 42.67 MHz/T, for hydrogen). The net magnetisation can be brought out of its equilibrium position by applying a RF pulse. A RF pulse is a magnetic field applied perpendicular to the external magnetic field and matching the Larmor frequency. The strength and duration of the RF pulse determines the flip angle of the magnetisation according to:

$$\theta = \gamma \cdot B_1 \cdot \tau, \tag{3.2}$$

with $\theta$ the flip angle, $B_1$ the strength of the RF pulse and $\tau$ the duration of the RF pulse.

After turning off the RF pulse the spins return to their original alignment. The magnetisation precessing at Larmor frequency in the x-y plane induces a current in a coil positioned parallel to $B_0$ (Figure 3.2), this is the MR signal we measure. At time t=0, the moment the RF pulse is turned off, the signal is at maximum and then decays according to:

$$FID = e^{-t/T_2^*} \cdot \cos(\omega \cdot t), \tag{3.3}$$

with FID the Free Induction Decay, $\omega$ the precessing frequency and $T_2^*$ a relaxation time, which will be discussed in the next section.

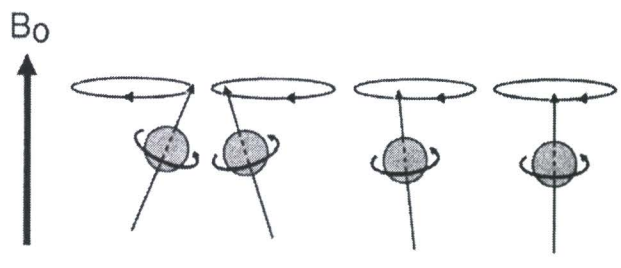


*Figure 3.1: Spins precessing in an external magnetic field $B_0$ [9]*

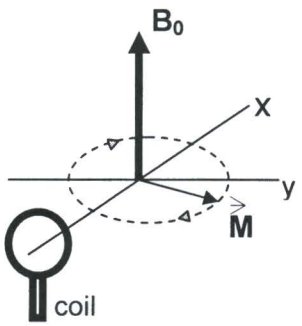


*Figure 3.2: Precessing magnetization ($\vec{M}$) induces current in a coil.*

To create an image, information is necessary about where the signal is coming from in the body. This process is called spatial encoding and it requires the use of gradients, which are additional magnetic fields that are linearly dependent on the position. This results in a position dependent Larmor frequency. Gradients, created by gradient coils, are used for position encoding in three dimensions.

### 3.1.1 Relaxation times $T_1$, $T_2$ and $T_2^*$

The term relaxation refers to the spins relaxing back to their equilibrium state. Relaxation times are inherent properties of tissues. $T_1$ is called the longitudinal- or spin-lattice relaxation time because it refers to the time it takes the spins to recover the initial longitudinal magnetisation ($M_0$). During this recovery the spins transfer the energy they obtained from the RF pulse to the surrounding lattice. The rate at which the z-component of the magnetisation ($M_z$) recovers to the initial magnetisation ($M_0$) is given by:

$$M_z(t) = M_0 \cdot \left(1 - e^{-t/T_1}\right) \tag{3.4}$$

$T_2$ is the transverse- or spin-spin relaxation time. It describes the decay of the transverse magnetisation vector $M_{xy}$ according to:

$$M_{xy}(t) = M_0 \cdot e^{-t/T_2} \tag{3.5}$$

The transverse relaxation occurs primarily due to spin-spin interactions, which cause the spins to dephase partially. The transverse relaxation occurs 5 to 10 times faster than the longitudinal recovery. Inhomogeneities in the external magnetic field increase the dephasing, resulting in an even shorter relaxation time, called $T_2^*$. $T_1$ recovery, $T_2$- and $T_2^*$ decay are drawn together in Figure 3.3.

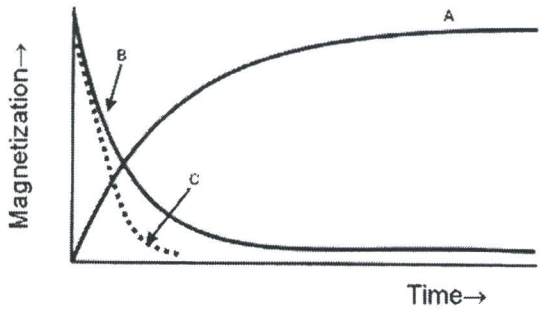


*Figure 3.3: $T_1$ recovery (A) versus $T_2$ and $T_2^*$ decay (B and C, respectively) [9]*

### 3.1.2 Pulse sequence

The steps of basic hardware activity incorporated in a pulse sequence are schematic illustrated in a time diagram. Along the horizontal axes the time during the execution of the sequence is indicated. Each line in the diagram represents a different hardware component. The first line denoted by RF is for the radio frequency transmitter. Subsequently there is a line for each gradient ($G_s$ = slice selection gradient x, $G_\phi$ = phase encoding gradient y, $G_f$ = frequency encoding gradient z, also called readout gradient). All three gradients give spatial information for one of the three dimensions. Finally a line is added for the recorded signal (s).
Figure 3.4 shows the timing diagram of the Spin Echo, the most frequently used pulse sequence. The first RF pulse is a 90° pulse, which flips the magnetisation over an angle of 90°. The second RF pulse is a 180° pulse at time TE/2 used for rephasing the spins. The slice selection gradient is turned on during both RF pulses, to make sure these pulses are experienced by the right set of spins. The phase encoding gradient is increased gradually each time the cycle is repeated.

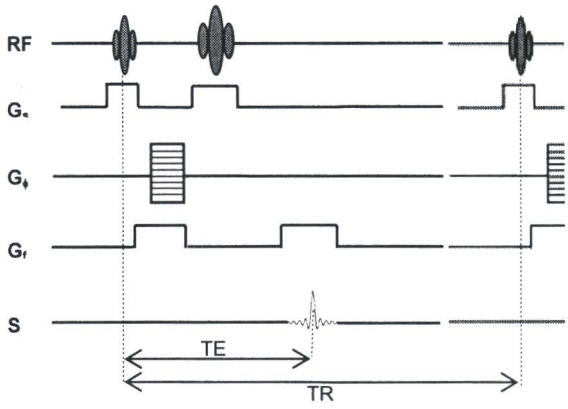


*Figure 3.4: Time diagram of Spin Echo*

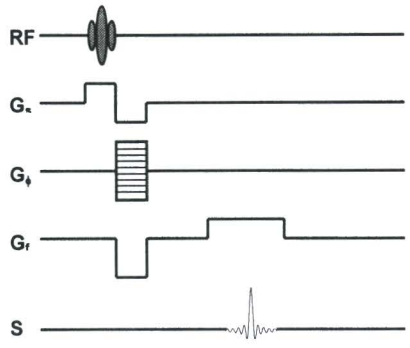


*Figure 3.5: Time diagram of Gradient echo*

Echo time (TE, see Figure 3.4) is defined as the time between the 90° RF pulse and the measurement of the maximum signal. Another time of interest is the repetition time (TR), defined as the time after which the cycle is repeated. TE and TR together with the earlier mentioned relaxation times $T_1$, $T_2$ and $T_2^*$ are the major factors in MRI that determine the contrast in an image. Table 3.1 summarizes the image weighting factors for Spin Echo images.
Figure 3.5 shows the timing diagram of the Gradient Echo pulse sequence. The RF pulse is usually a 90° pulse. The slice selection gradient shows both a positive and a negative lobe. The first is for the slice selection and the second for rephasing of the spins. Again, the phase encoding gradient is increased gradually each time the cycle is repeated. The frequency encoding gradient provides us with the spatial information during read out.

| | **Short TE** | **Long TE** |
|---|---|---|
| **Short TR** | $T_1$-weighted | Mixed contrast |
| **Long TR** | Proton density weighted | $T_2$-weighted |

*Table 3.1: Image appearance as a function of TR and TE for Spin Echo images.*

Another name for Gradient Echo is Field Echo and used with a short TR ($TR \approx T_2$) and a flip angle < 90°, it is called Fast Field Echo (FFE). FFE can be performed in different varieties and is mostly used for Magnetic Resonance Angiography (MRA), which will be discussed in more detail in the next section. Various other pulse sequences are possible with different features and advantages, e.g. the (fast) spin echo and echo planar imaging. For more information about these techniques I will refer again to the earlier mentioned textbooks [24 – 26].

## 3.2 Magnetic Resonance Angiography

The term Magnetic Resonance Angiography (MRA) describes a variety of MRI methods used to image blood vessels. Currently 3 methods for MR Angiography are frequently used: time-of-flight (TOF) techniques, Contrast Enhanced MRA and phase-contrast angiography (PCA). The first two methods will be briefly discussed before we go into more detail about PCA.

### 3.2.1 Inflow (Time Of Flight) techniques

Time-of-flight angiography is based on the Spin Echo sequence. The basic principle is that the 90° and 180° pulses are given in different slices, by the use of different slice selection gradients. These gradients have to be chosen in such a way that the flowing blood experience both RF pulses. With the proper choice of TE (Table 3.1), blood will appear bright, while the static tissue appears dark, since it does not experience both pulses.

### 3.2.2 Contrast enhanced MRA

When a paramagnetic contrast agent (for example gadolinium) is injected into the blood the $T_1$ relaxation time of the fluid in the blood vessels is reduced. When the data is collected using pulse sequences with a short TR value, the signal contribution of the surrounding tissues is negligible, due to their relative long $T_1$, whereas the blood with shortened $T_1$ will give a large contribution. This technique produces high quality imaging but it requires injection of the contrast fluid in the patient. Furthermore it is not useful quantitative flow information.

### 3.2.3 Phase Contrast MRA

Phase contrast MR Angiography (PCA) is based on the fact that the phase (Φ) obtained by flowing blood through a gradient is proportional to its velocity (v). The most common method for PCA is by the use of bipolar gradients (figure 3.4 a). This process is called flow encoding. Because the two lobes in the bipolar gradient have equal area, the second gradient rephases the effect of the first and no net phase change is observed by stationary tissues (figure 3.4 b) However flowing blood will experience a net phase (Φ) shift proportional to its velocity (v, assuming constant flow velocity):

$$\phi = \int \omega \cdot dt = \int (\gamma \cdot G \cdot v \cdot t) \cdot dt = \frac{1}{2} \cdot \gamma \cdot G \cdot v \cdot t^2 \qquad (3.12)$$

The pulse sequence for PCA is similar as the one for Gradient Echo, with bipolar gradients added between the RF pulse and the phase encoding gradient.

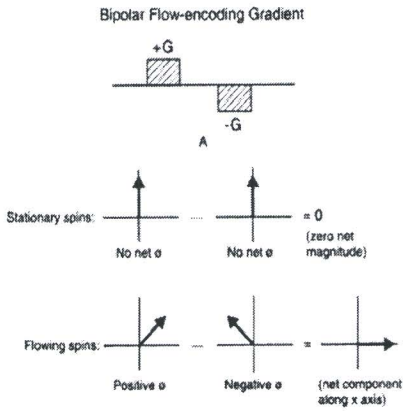


*Figure 3.4: A bipolar flow-encoding gradient (A) induces no phase change in stationary spins and a net phase change proportional to their velocity in flowing spins (B) [9]*

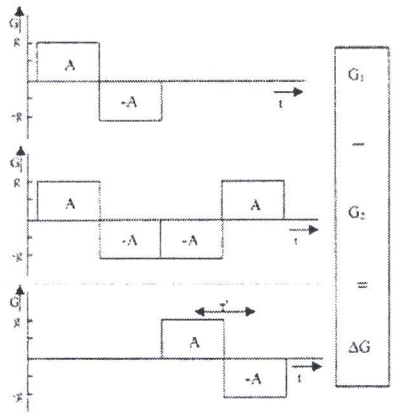


*Figure 3.5: Example of a biplor gradient (bottom) constructed by subtraction of two other gradients (top).*

A single measurement is not sufficient for quantitative assessment of the velocity since phase shift depends not only on the gradient, but also on field inhomogeneities. To cancel out the field inhomogeneities a method called phase difference method is used. With this method two measurements are done with different gradients $G_1$ en $G_2$, chosen in such away that subtraction leads to a bipolar gradient $\Delta G$ (Figure 3.5):

$$\Delta G = G_1 - G_2 \qquad (3.13)$$

The resulting phase difference ($\Delta\phi$) depends on the gradient alone, no longer on the field inhomogeneities, and is directly proportional to the velocity of the blood flow. Since $\Delta\phi$ is defined between $-\pi$ and $\pi$, the maximum velocity that can be measured is determined by $\Delta G$ and can be chosen as a parameter when performing a MRI scan. This parameter is called $v_{enc}$ (velocity encoding value). Choosing $v_{enc}$ to low will lead to aliasing, which will be discussed in the next section.

The blood velocity can be calculated by:

$$v = \frac{\Delta\phi}{\pi} \cdot v_{enc} \tag{3.14}$$

The two measurements with different gradients result in two different signals, $S_1$ and $S_2$, which can be represented as vectors:

$$S_x = A_x \cdot e^{i\phi_x}, \tag{3.15}$$

with A the amplitude, $\phi$ the phase and x = 1 or 2. From these vectors various images can be constructed. For this research the FFE/M (Fast Field Echo / Modulus) and the PCA/P (Phase Contrast Angiography / Phase) are important. The FFE/M image gives anatomical information and is defined as the mean of the amplitudes of both signals:

$$\text{FFE/M:} \quad \frac{|S_1| + |S_2|}{2} = \frac{A_1 + A_2}{2} \tag{3.16}$$

The PCA/P image is used to gain quantitative flow information and defined as the phase difference between the two signals:

$$\text{PCA/P:} \quad \phi_1 - \phi_2 = \Delta\phi \tag{3.17}$$

Examples of phase and amplitude images will be shown in the next chapter.

## 3.3 Artifacts and limitations

There are several factors affecting the accuracy of the PCA technique. The most important for this research aliasing, misalignment and partial volume effects, will be discussed in this section.

### 3.3.1 Aliasing

Because the nature of phase is cyclic, there is a natural limitation to the measurement range of 2 $\pi$ radians (between -$\pi$ and $\pi$). Therefore the velocity measurement, which is directly related to the phase, is similarly limited. An absolute phase shift larger than $\pi$ will be recorded as a phase shift between -$\pi$ and $\pi$. In the constructed image this can lead to white spots blood vessels that should appear dark (Figure 3.6).
With the right choice of $v_{enc}$, larger than the maximum measured velocity, aliasing can be prevented.

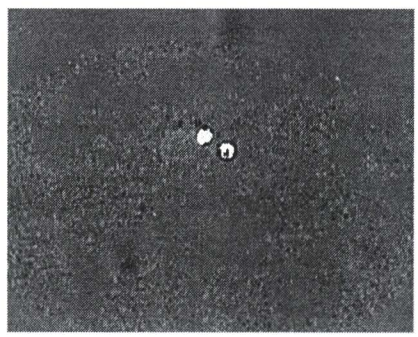

*Figure 3.6: Example of aliasing in a PCA image*

### 3.3.2 Misalignment

When in a PCA image the chosen slice is not perpendicular to the blood flow of interest, misalignment occurs. This introduces an error in the measured flow and cross sectional area. The relation between the measured flow ($F_{meas}$) and true flow ($F_{true}$) is relatively simple:

$$F_{meas} = \cos\theta \cdot F_{true}, \tag{3.18}$$

with $\theta$ the angle of misalignment. Generally $\theta$ is of the order 5°, causing an error of less than 1%.

### 3.3.3 Partial volume effects

Since the pixels in an image can not be made infinitely small, it is possible that at the edge of a blood vessel the signal in one pixel has contributions of both stationary and moving spins. This is called partial volume effect. It is most apparent for small vessels. Due to different relaxation times of blood and the surrounding tissues, the phase of the moving spins has a larger influence on the measured $\Delta\phi$ than the phase of the stationary spins. This can lead to overestimation of the velocity in edge pixels. However the velocity at the vessel wall is small (see chapter 2) and the effects can be neglected, unless the pixel size is large compared to the vessel diameter.
Furthermore it is difficult to determine the exact location of the vessel wall, due to partial volume effects. Again, the error is small when the pixels are made small enough.

### 3.3.4 Turbulence

If turbulence occurs in the blood flow, an error is made in measuring the velocity with the PCA technique. Due to the turbulence the velocity in one pixel is not distributed homogeneous, in both magnitude and direction. This results in a smaller signal if we sum all spins together.

# 4. Materials and methods

This chapter describes the materials and methods used for obtaining images, vessel detection and analysis. The vessel detection and analysis methods are implemented in Mathematica © (version 5.0, Wolfram Research).

## 4.1 Imaging Methods

In the previous chapter the basic principles of MRI were discussed. Here we will discuss in more detail the protocols for obtaining the images we used for analysis.

### 4.1.1 Retrospective study with endurance athletes

In this study 14 endurance athletes were examined, 9 patients and 5 controls. Patients were selected based on their determined vascular problems. All patients showed kinking at hip flexion and intravascular damage. The controls were endurance athletes with no complaints or possible vascular problems.
The images were made with a standard whole body scanner (Philips Gyroscan NT 1.0T, Figure 4.1) using a Synergy Body Coil (Figure 4.2) for signal detection. First a TOF angiogram was acquired and used for further planning (Figure 4.3) The quantitative flow scans were made at 3 locations: 2 cm below aorta bifurcation, 2 cm below iliac bifurcation and 2 cm above femoral bifurcation. All three locations were measured in two positions: stretched legs and flexed hips, but only the images with stretched legs were usable for further analysis. The scans were implemented as a $T_1$-FFE sequence with the following scan parameters: TR/TE/$\alpha$=15/9/20°, FOV 256 mm (RFOV 70%), Matrix size 256, slice thickness 7 mm. Velocity encoding is done perpendicular to the chosen slice. The velocity encoding parameter, $v_{enc}$ is chosen 100 cm/s or 125 cm/s in the patient images. Both values appeared to be to small in most patients and controls.

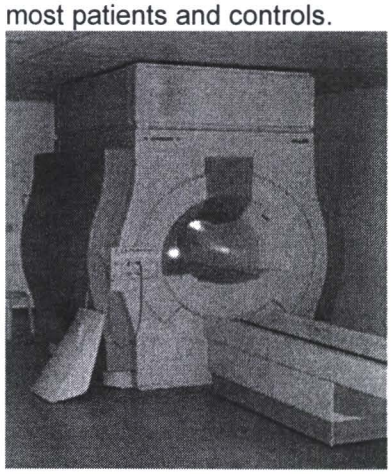

*Figure 4.1: Philips Gyroscan NT, 1.0 T*

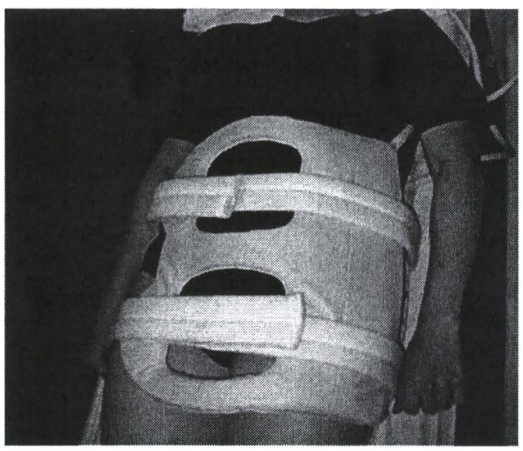

*Figure 4.2: Synergy body coil positioned on a volunteer*

### 4.1.2 Volunteer study

This study was done to investigate the influence of the way of planning MRI scans on the measured velocity, flow, diameter and cross-sectional area in a quantitative flow image. Also the variability in these parameters between different heart beats is tested for. Four volunteers, with no history of endurance sports, were examined.
The images were acquired with the same equipment as mentioned in the previous section (Section 4.1.1, Figure

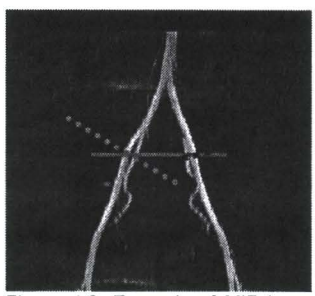

*Figure 4.3: Example of MIP image and planes of planning for different PCA images in volunteer study*

4.1 and 4.2). After a first survey scan an inflow san was made to create MIP (Maximum Intensity Projection) images (Figure 4.3). These images are used to plan the 5 series of PCA images, for the actual analysis. Only one location (2 cm below iliac bifurcation) in one position (stretched legs) is measured. The first series were planned as perpendicular as possible to both vessels (straight line in Figure 4.3). This method of planning will further be denoted as the MMC-classical method, since this is still the most commonly used method in the Máxima Medical Centrum. Three series were made with exactly the same planning to investigate the variability between different heart beats. The fourth en fifth series were planned perpendicular to the right and left (dotted lines) external iliac artery, respectively. This method will be further denoted as the perpendicular method. The scans were again implemented as a $T_1$-FFE sequence with the following scan parameters: TR/TE/$\alpha$=14/8.8/20°, FOV 256 mm (RFOV 70%), Matrix size 256, slice thickness 7 mm. The velocity encoding is done perpendicular to the slice and $v_{enc}$ = 200 cm/s for all volunteers in first instance. Some volunteers appeared to have much lower velocity and $v_{enc}$ was reduced to 150 cm/s. The images acquired in this study were only analysed with the active shape segmentation method, as will be described in section 4.2.3.
To be able to calculate arterial stiffness as described in section 2.3 blood pressure measurements are needed. After the MRI scans the blood pressure on both arms and ankles was measured at the volunteers, while they were still lying down. A full automatic sphygmomanometer was used. With these blood pressure measurements we can calculate the compliance and distensibility coefficient as described in section 2.3, Formula 2.14 and 2.15. For the pulse pressure ($\Delta$P in the heart phase) at the external iliac arteries we use the mean of the pulse pressure measured at the arm and at the ankle. The area change ($\Delta$A) is the difference between maximum and minimum area in a heart phase. The relative area change is $\Delta$A/A, with A the mean area during the diastole.

## 4.2 Methods of vessel detection

As mentioned in the previous chapter (3.2.3), MR images made with the PCA technique produce anatomical images (amplitude, FFE/M) and quantitative flow (QF, PCA/P) images (phase) simultaneously. Figure 4.4 (a) and (b) show the amplitude and phase image respectively. In this example the blood vessels during systole are well recognizable in both phase and amplitude image.

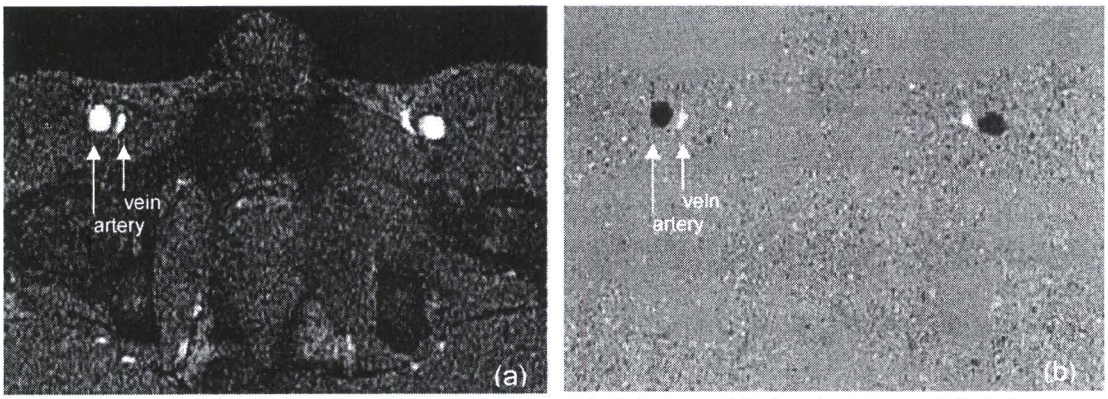


*Figure 4.4: Images made with the PCA technique. (a) The magnitude image and (b) the phase image, indicated are the artery (during systole) and vein, 2 cm above femoral bifurcation*

To obtain information about the velocity of the blood and the changes in shape of the vessel during a heart cycle all phase and amplitude images were imported in Mathematica. The algorithm is set up in such a way that it first automatically detects the artery of interest from the amplitude image and then uses these coordinates to

extract information from the phase image, since the arteries are not visible in all phase images.
Various methods are available for vessel detection; three of the most promising will be discussed. The first method uses a threshold to detect vessels and erosion and dilation for removing the structures that do not belong to the vessels of interest. The second method is based on contour detection, drawing contours through points with matching grey levels. Both the grey levels of the original anatomical image and the so called Gaussian derivatives are used. The final method discussed in this section is called active shape segmentation. A shape (e.g. a circle) starts growing or shrinking from the inside or outside the vessel and stops when it reaches the border.

### 4.2.1 Threshold, erosion and dilation

In all anatomical images, the vessels appear white. A threshold selects all the coordinates with a grey level above a certain value. Since not all image series are of the same quality, this threshold value has to be adapted manually for each patient. A standard threshold value calculation (e.g. using a threshold value at ½ maximum), did not work in this study, due to the large variability in image quality.
Not only arteries but also veins, fat and some other tissues appear white on the amplitude images. To ensure that only the vessel of interest is selected, a target area is manually defined in one image of the series. After the threshold procedure, only the part inside this target area is used for further analysis. The threshold procedure is depicted in Figure 4.5.

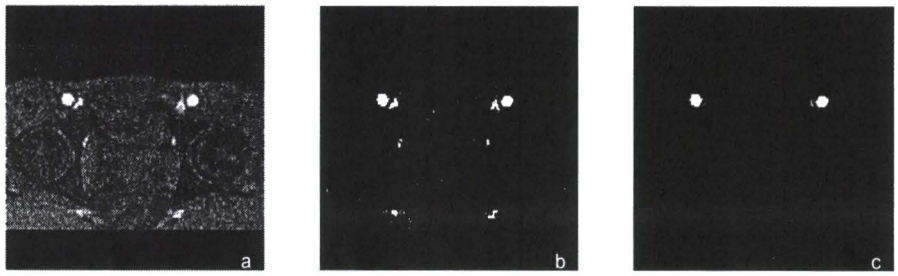


*Figure 4.5: (a)The original image, (b) the selected coordinates after threshold and (c) the selected coordinates in the target area.*

The detected vessels as shown in Figure 4.5 c appear to be correct, but there is still some noise. Erosion and dilation are used for more precise detection of the arteries of interest. Erosion and dilation are both basic morphological operations and described in more detail in [27]. Mathematical morphology is a tool for extracting image components that are useful for representation and description of regions. Before these techniques can be understood, some basic mathematical definitions are needed.
Let $A$ and $B$ be sets in $Z^2$, with components a = ($a_1$, $a_2$) and b = ($b_1$, $b_2$), respectively, $B_x$ the translation of $B$ by $x$ and $\hat{B}$ the reflection of $B$ around the centre.
Then the erosion of $A$ by $B$ is defined as:

$$A \ominus B = \left\{ x \middle| (B)_x \subseteq A \right\} \tag{4.1}$$

In words; the erosion of $A$ by $B$ is the set of all points $x$ such that $B$, translated by $x$, is contained in $A$. Set $B$ is usually referred to as the structuring element.
The dilation of $A$ by $B$ is defined as:

$$A \oplus B = \left\{ x \middle| \left(\hat{B}\right)_x \cap A \neq \emptyset \right\} \tag{4.2}$$

In words; the dilation of $A$ by $B$ is the set of all $x$ displacements such that $\hat{B}$ and $A$ overlap by at least one nonzero element.

There are some variations known on the above equations for erosion and dilation. The ones mentioned here are usually favoured in practical implementations of morphology. The actual effect of erosion and dilation is shrinking and expanding the image respectively.
Erosion is used here to remove the little spots around the actual artery. Dilation is then used to reconstruct the artery without the artefacts. Dilation is necessary since in the erosion process also parts of the artery are removed. This is shown in Figure 4.6, for the same patient as shown in Figure 4.5. The final result is a set of coordinates defining all the pixel corners within and at the edge of a vessel.

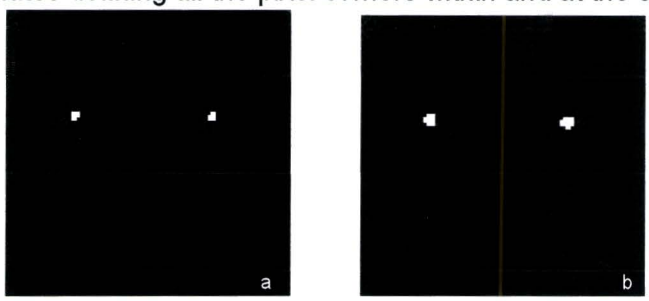


*Figure 4.6: Image of figure 4.5 (c), (a) after erosion and (b) after*

### 4.2.2 Contour detection and Gaussian Derivatives

Contour detection is a pre-programmed operation in Mathematica, which connects identical grey values in a picture. It could be used directly on the amplitude image to find the edge of the blood vessel by connecting identical grey values. For some pictures this works very well (Figure 4.7 a), but in a lot of cases the images are not accurate enough and wrong contours will be detected (Figure 4.7 b).

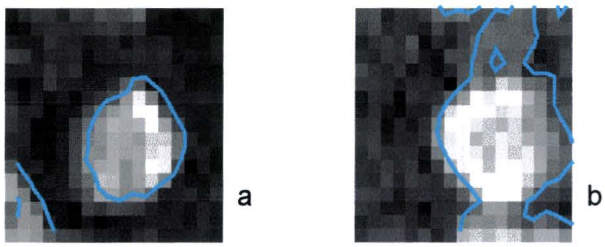


*Figure 4.7: Example of an image where detection of the vessel on basis of identical grey values in the amplitude image a) does work and b) does not work.*

Convolution of the so-called Gaussian derivative kernel with the image produces gradient images, which are more suitable for contour detection and will be used here to detect the blood vessels. Since blood vessels appear white (or light grey) in a dark environment on the MRI-images there is a maximum in the gradient of the image at the border of a blood vessel. A maximum in a gradient can be determined by the zero crossings of the *Laplacian* ($\Delta$). That is what we will use here.

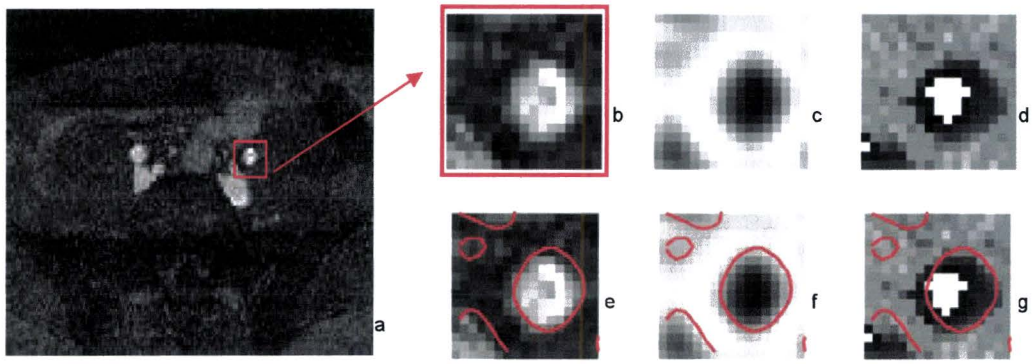


*Figure 4.8 Detection of blood vessels with Gaussian derivatives: a) the original image, b) area of interest, c) second Gaussian derivative plot of b, d) corresponding quantitative flow image, e) Anatomical image with contours at zero-crossing of second Gaussian derivative, f) the contours of zero-crossing of second Gaussian derivative in the derivative image, g) as e and f in QF image*

Figure 4.8 shows the second Gaussian derivatives (Gaussian Laplacian) image and the contour at zero crossing as detected by Mathematica.
From the detected contours edge points can be extracted and with Mathematica all the pixels within the contour can be found resulting again in a set of coordinates of all the pixel corners within and at the edge of a vessel.
This detection method is based on scale space theory. A short introduction on this subject will be given here, a detailed description can be found in the Front-End Vision book [28]. Scale space theory is the theory of apertures through which we and machines observe the world. To extract information from image data, we need an operator to interact with the data. Various derivations were made to find this operator, all leading to the Gaussian Kernel [28]:

$$g(x;\sigma) = \frac{1}{\sqrt{2\pi\sigma^2}} e^{-\frac{x^2}{2\sigma^2}}, \tag{4.3}$$

with $\sigma$ the width of the kernel, in scale space theory shortly denoted as scale. Equation 4.3 gives the Gaussian kernel in 1 dimension, but it can easily be extended to N dimensions. When we take spatial derivatives (with respect to x) of the Gaussian kernel repetitively, we see a pattern emerging. Every next derivative consists of *Hermite polynomials* of increasing order, multiplied with the original Gaussian function. The order of the Hermite polynomial equals the order of differentiation and also the number of zero crossings of the derivative.
The effect of convolution of the Gaussian kernel with a test image (Figure 4.10 a) can be seen in Figure 4.10 b, the image is blurred and the edges are smoothed. The second order derivatives in x- and y-direction are shown in Figure 4.10 c and d respectively. Finally the Laplacian as used in this report is shown in Figure 4.10 e.

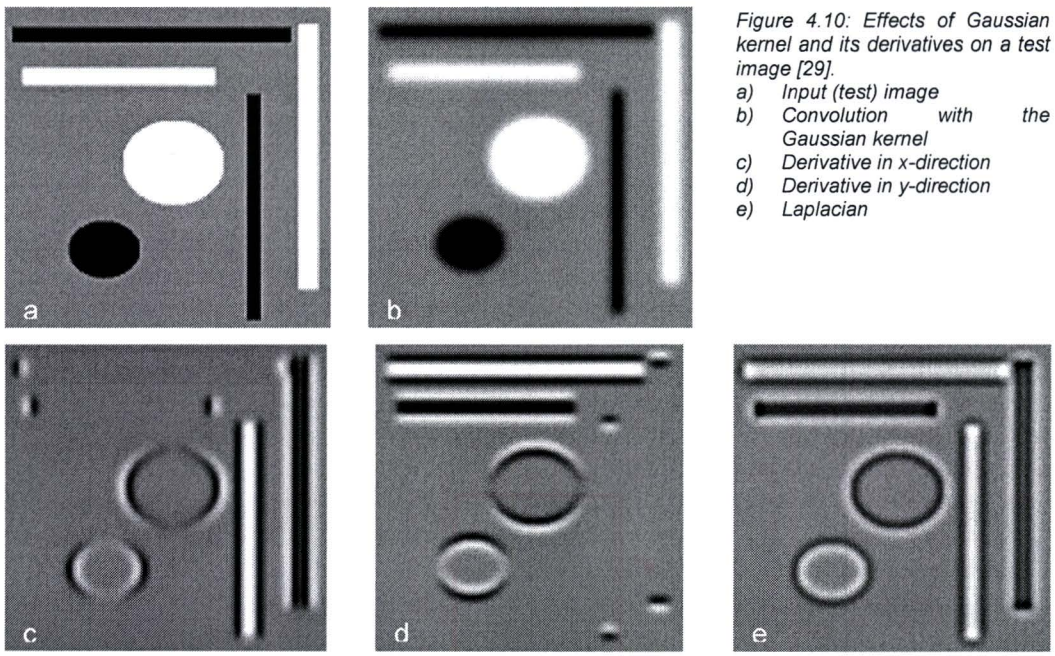


*Figure 4.10: Effects of Gaussian kernel and its derivatives on a test image [29].*
*a) Input (test) image*
*b) Convolution with the Gaussian kernel*
*c) Derivative in x-direction*
*d) Derivative in y-direction*
*e) Laplacian*

In this example the edge detection by connecting equal grey-levels in the Laplacian works well, since there is a large difference in greyscale between the blood vessel and the surrounding tissue. Unfortunately this is not the case in all the images. An example of an image where this detection method does not work, because another bright structure appears close to the artery, is given in Figure 4.9.

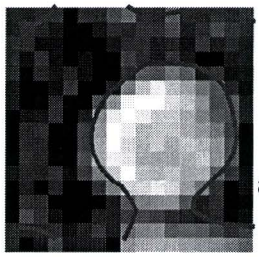

a

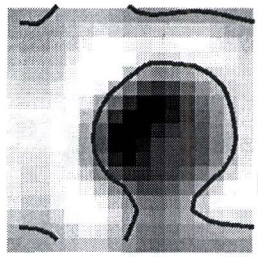

b

*Figure 4.9: Example of an image where the described detection method does not work, due to a low gradient in the grey scale at part of the vessel wall. a) The original anatomical image. b) The second Gaussian derivative image.*

### 4.2.3 Active Shape segmentation

Active shape segmentation is based on a theory first introduced by Kass et al. [30]. The active shape can be compared to an elastic band, which is stretched out and wants to contract back to its original shape, against a force. The shape, mostly called snake or contour, is the elastic band and the force is derived from the image or a derivative of the image. Force equilibrium between the internal forces of the contour and the external forces of the image gives the desired solution. The starting position of the contour has to be placed nearby the image feature, e.g. an edge, which has to be detected.

When we choose a parametric representation $V(s)=(X(s),Y(s))$, the movement of the contour under influence of forces can be represented as [31]:

$$\gamma \frac{\partial V}{\partial t} = F_{ext}(V) + F_{\text{int}}(V), \tag{4.4}$$

with $\gamma$ a constant which can be used to control the importance of the image features, $F_{ext}$ the external forces and $F_{int}$ the internal forces working on the snake, given by the following equations:

$$F_{ext}(V) = -\gamma \cdot \nabla G_{\sigma}(x,y) * I(x,y) \tag{4.5}$$

$$F_{\text{int}}(V) = \frac{\partial}{\partial s}\alpha(s)\frac{\partial V}{\partial s} - \frac{\partial^2}{\partial s^2}\beta(s)\frac{\partial^2 V}{\partial s^2} \tag{4.6}$$

$G_{\sigma}(x,y)$ is the earlier mentioned Gaussian kernel, $I(x,y)$ represents the image, $\alpha$ and $\beta$ are parameters to control the continuity (equidistance of the parameterization points) and curvature (rigidity) of the contour respectively. Various other representations of active contour models are available in literature. Advantage of this representation is that additional forces can simply be added in equation 4.4.

Implementation of this technique in Mathematica has been performed by Panday [31]. Most of his algorithm is copied and adapted for the images in this study. The major difference with Panday's method is the image on which the snake operates. He used the gradient magnitude image, while in this research it was chosen to let the snake operate on the inverse of the Gaussian Laplacian of the image, since the edges of the blood vessel are more distinct in this image. Furthermore his goal was to detect organs in MRI images of a mouse, while this research is concentrated on detecting arteries in MRA images of endurance athletes.

As starting position of the snake 20 parameterization points in a circle or ellipse are manually defined in the neighborhood of the vessel wall. The algorithm checks for every point if there is a neighboring point with a lower value. If a lower value is found nearby, the point will move to that value. This process is repeated until the points stop moving. The maximum number of steps for the snake is set to 101.

For most images the best results were acquired with $\alpha$ = 0.35, $\beta$ = 0.65 and $\gamma$ = 1.5. In some exceptional cases these parameters had to be manually adapted to be able to detect the contour. Panday [31] showed the effect of varying the parameters, to

extreme values (e.g. zero). This results in a snake, with extreme shapes or no movement of the snake at all. The choice of the parameters in this research was done by trial and error. The detection of a vessel wall by active snake in 3 steps is shown in Figure 4.11. The number of steps needed for detection depends strongly on the image quality and the definition of the starting position.

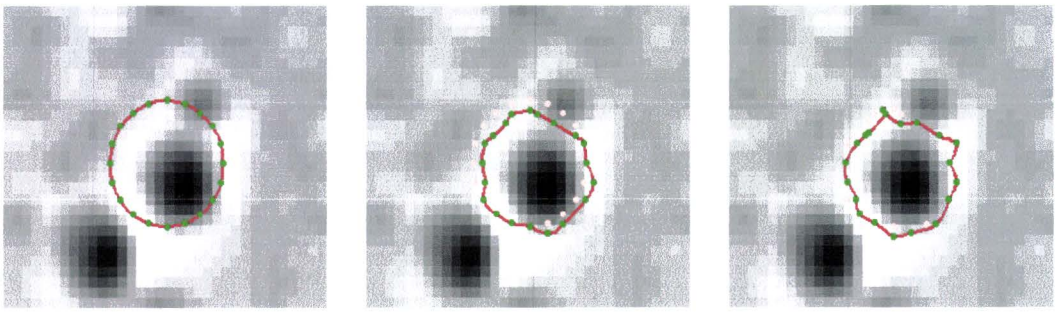

*Figure 4.11: Detection of the vessel wall by the Active Snake method. The green dots denote the new coordinates per step, while the pink dots denote the starting coordinates from the previous image*

Projection of the result (right image in Figure 4.11) on the anatomical and velocity image shows the detection (Figure 4.12).

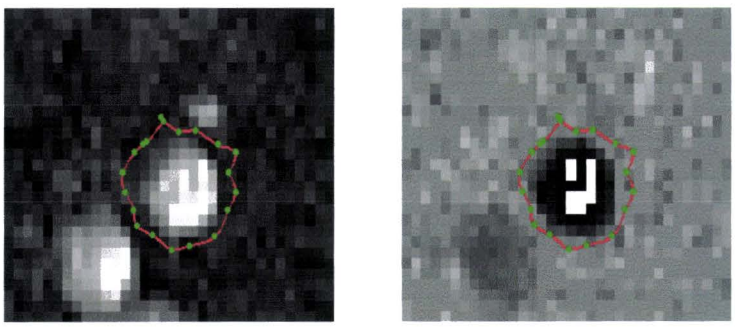

*Figure 4.12: Projection of the snake result of Figure 4.11 on the anatomical (left) and velocity image (right)*

The post processing following the active snake method is similar as described for contour detection in the previous chapter. First the end points of the snake are rounded to integer coordinate values and then the internal coordinates are determined.

## 4.3 Analysis

Following detection of the vessels, parameters of interest have to be extracted. All described segmentation methods result in a set of coordinates. These coordinates can be used to obtain the relevant information from the quantitative flow image.

### 4.3.1 Diameter

If a circle is fitted through the detected vessel, the radius of this circle is a good approximation of the radius of the vessel. The radius of this circle can be calculated by taking the mean of all distances between the centroid (red dot in Figure 4.13) and the edge coordinates of the vessel (denoted as green lines in Figure 4.13).

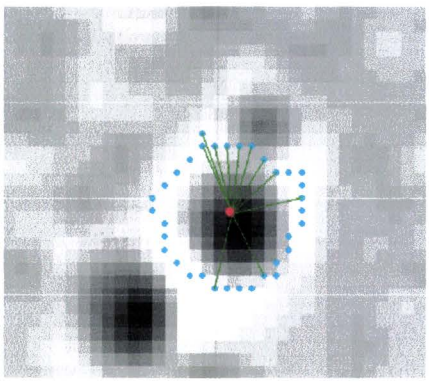

*Figure 4.13: Schematic representation of diameter determination.*

The centroid ( $\bar{\mathbf{x}}$ ) of the detected vessel area is calculated by [32]:

$$\bar{\mathbf{x}} = \frac{\sum_{i=1}^{n_{edge}} \mathbf{x}_i}{n_{edge}}, \tag{4.8}$$

with $\mathbf{x}_i$ the set of edge coordinates. The approximated vessel diameter (D) is now calculated by:

$$D = 2 \cdot \frac{\sum_{i=1}^{n_{edge}} (\mathbf{x}_i - \bar{\mathbf{x}})}{n_{edge}}, \tag{4.9}$$

### 4.3.2 Cross sectional area

In the total set of coordinates, resulting from segmentation, both internal and edge coordinates are included. The edge coordinates (cyan dots in Figure 4.13) can be determined with Mathematica command RegionBorder. The coordinates define corners of pixels. If we should simply multiply the total number of coordinates ($n_{tot}$) with the area of one pixel ($a_{pixel}$) an error is introduced, because the border pixels contain partly "outside" information. A more accurate approach is given by:

$$a_{vessel} = \left(n_{total} - \tfrac{1}{2} n_{edge}\right) \cdot a_{pixel}, \tag{4.7}$$

with $a_{vessel}$ the cross sectional area of the vessel and $n_{edge}$ the number of edge pixels. In this research all the images have a pixel area of 1 $mm^2$.

### 4.3.3 Velocity

The gray level in the QF image is directly proportional to the velocity and thus the velocity can easily be extracted from the images, with the coordinate sets left after segmentation.
The parameter of interest in the velocity determination is the peak systolic velocity. Just taking the maximum of all velocities in all pixels during the heart phase is not very reliable since this maximum could be an outlier. Therefore we have chosen to calculate in each image the mean velocity of the ten pixels with the highest value. And determine the peak systolic velocity by taking the maximum of these means in a heart phase. The number of ten pixels is not chosen arbitrarily, but can be derived if we assume plug flow in the arteries. This derivation is explained in Appendix 2.

### 4.3.4 Flow

Finally the velocity data can be used to calculate the flow according to:

$$F = a_{pixel} \cdot \sum_{i=1}^{n_{total}} v_i, \tag{4.10}$$

with $v_i$ the velocity in pixel $i$.

### 4.3.5 Analyzed parameters as a function of the heart phase

Figure 4.14 shows the measured cross sectional area, diameter, velocity and flow as a function of the heart phase, for one patient in the external iliac artery. More results will be shown and discussed in the next chapter.

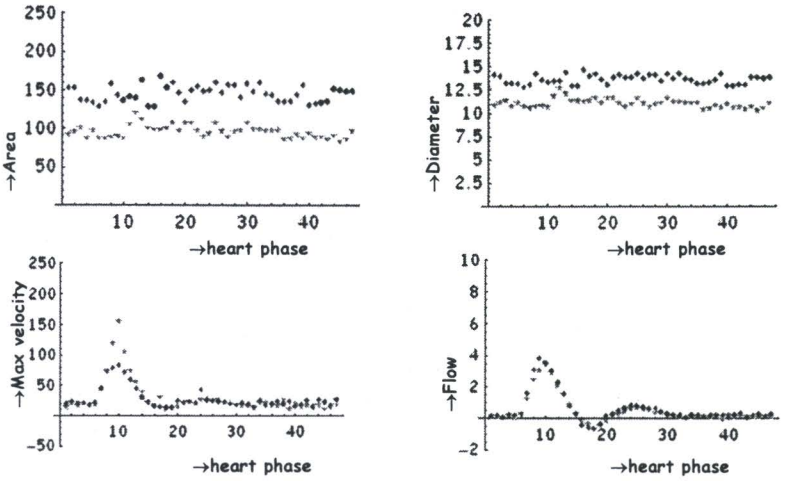


*Figure 4.14: Example of information extracted from the QF images during one heart phase of one patient. On the horizontal axes the image in the heart phase is denoted and on the vertical axes*
*a) Cross sectional area ($mm^2$)*
*b) Diameter (mm)*
*c) Maximum velocity (cm/s)*
*d) Flow (l/min)*
*Information for iliac arteries in both legs is shown:*
*= Left leg (pathological)*
*= Right leg*

# 5 Results and discussion

In the previous chapters the methods of image acquisition and processing were discussed. This chapter will present the results of the various studies that were done as parts of this research. First the different methods of automatic vessel detection will be discussed with all advantages and disadvantages. These detection methods were also compared with a manual detection method. The next section will deal with the results of the retrospective study on endurance athletes. Finally the results of the volunteer study will be presented.

## 5.1 Methods of vessel detection

Three segmentation methods for (semi-) automatically detection of the vessel have been presented in section 4.2. Two of them are worked out in more detail; the threshold-erosion-dilation method and the active snake method. The method of contour detection is not further investigated due to the poor results of the first try out. The two methods are compared to a third method: manual detection. Manual detection means manually detecting the contour by selecting points at the edge of the artery in each image of each series. This is a very time consuming detection method and subject to inter-observer variability. After presentation of the results, the different methods will be discussed. The advantages and disadvantages are weighed against each other and our choice for Active Shape as the preferential method is founded.

### 5.1.1 Results

Figure 5.1 shows the result of the different detection methods for one artery in one patient at one moment (Patient 1, right artery, image 10 / 47 in heart phase). The manual detection method and threshold, erosion and dilation were performed on the amplitude images, as shown in Figure 4.4 a. The Active Snake was performed on subsections of the images for the arteries of interest, as shown in Figure 4.8 b.

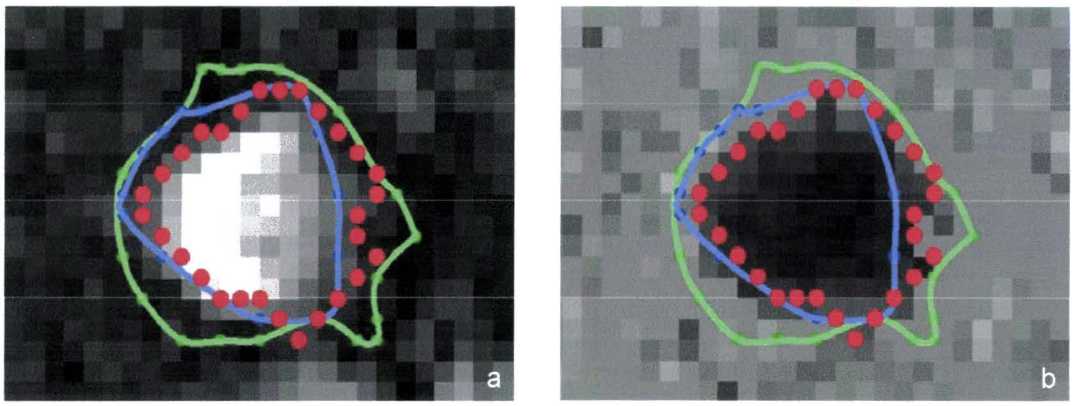


*Figure 5.1: Results of three segmentation methods for one artery, a) on the amplitude image, b) the result copied on the QF image. ——=Manual detection; ●=Threshold, erosion and dilation; ——=Active Shape method*

For one patient the arteries in one image series, acquired ~2 cm below the iliac bifurcation, were detected with all three methods. The resulting graphs displaying values for cross sectional area, diameter, maximum velocity and flow are shown in Figure 5.2. For flow and maximum velocity we observe similar shapes of the graphs and values of the same order. The graphs of the cross sectional area and diameter display only small variation during the heart phase. However comparing the values obtained using the three methods show a clear difference. The values for cross sectional area (further shortly denoted as area) and diameter measured by the active shape method are larger than measured manually or with the threshold method.

Note the difference between the left (pathological) and right external iliac artery in this patient in the maximum velocity.

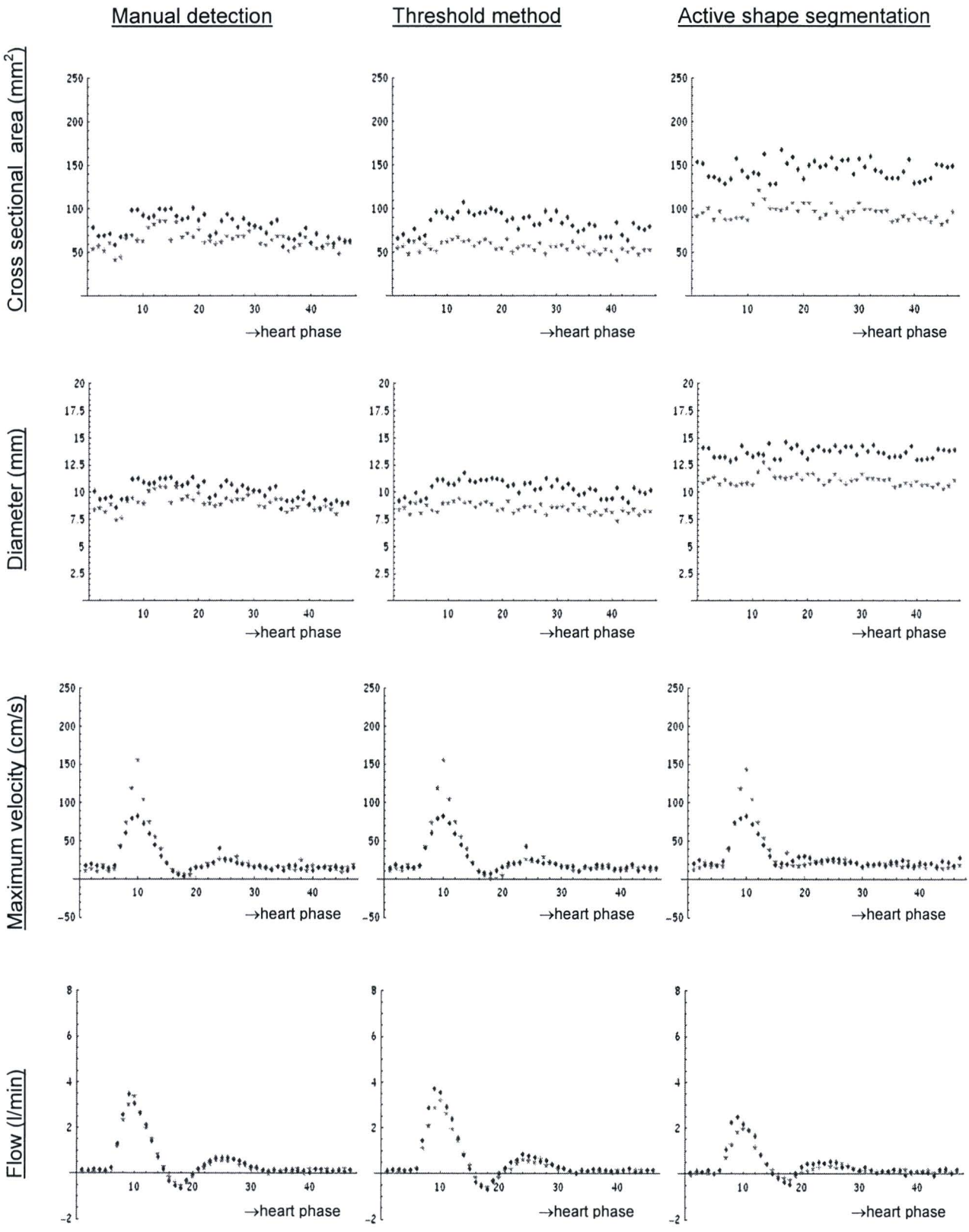


*Figure 5.2: Resulting graphs of three detection methods for patient 1.*

The threshold method and the active snake segmentation have been performed on all images of all patients. In the images of the controls and volunteers, the arteries were only detected by the active snake method.
To investigate the reproducibility of the three methods the mean and standard deviation ($\sigma$, see Appendix 4, Section 4) of the cross sectional area were calculated during diastole where we expect no more changes in the area. For these calculations we used the last 25% of the heart phase. The results for patient 1 are shown in Table 5.1.

| | Manual | Threshold | Active shape |
|---|---|---|---|
| **Left** | 57.50 ± 5.0 | 50.50 ± 3.8 | 88.79 ± 4.0 |
| **Right** | 66.00 ± 5.7 | 75.33 ± 7.5 | 141.58 ± 9.1 |

*Table 5.1: Mean and standard deviation for the cross sectional area during diastole of patient 1.*

From Table 5.1 several things can be observed. To start with the variation during diastole, the smallest relative variation is seen for the active shape method. Furthermore the values, presented in Table 5.1, obtained by the three methods show differences. The difference between the results obtained by using the manual method and using the threshold method are within the range of $2\cdot\sigma$. The values obtained by using the active shape method are larger than using the other two methods and this difference is no longer in the $2\cdot\sigma$ range. Another interesting observation of Table 5.1 is that using the manual technique the difference between left and right is smaller than $2\cdot\sigma$, whereas in the threshold method and active shape technique larger differences are observed.
For every patient the starting position of the snake in the active shape method is adapted manually to the shape and size of the vessel. Results of active shape segmentation with wrongly chosen starting positions are shown in Figure 5.3. Figure 5.3 a) shows a starting position not centred at the artery. The resulting snake is shown in Figure 5.3 b), the vessel is not detected. Figure 5.3 c) shows a starting position chosen too large, which results in detection of not only the external iliac artery, but the internal iliac artery was included with the snake too, Figure 5.3 d).

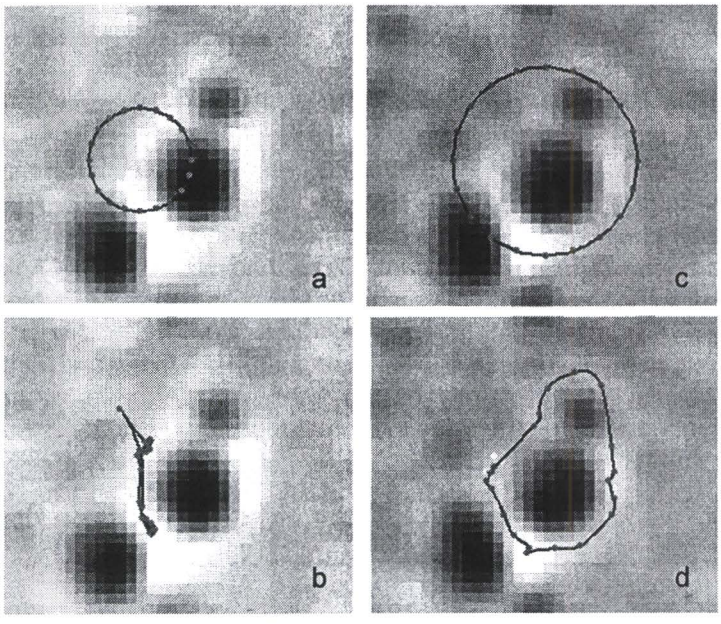


*Figure 5.3: Results of wrongly chosen starting positions in active shape segmentation. Images of patient one of the left external iliac artery; image 10 (a and b) and 12 (cand d) of 47 in heartphase.*
*a) Starting position chosen, not centered at the artery*
*b) Result after active shape segmentation with starting position a)*
*c) Starting position chosen to large.*
*d) Result after active shape segmentation with starting position c)*

### 5.1.2 Discussion

Threshold, erosion and dilation

The largest problem with this method is to define the right threshold value. In images with low contrast a low threshold is needed to be able to select the whole arteries in the region of interest. A low threshold value on the other hand can introduce a lot of noise, which cannot always be eliminated with erosion. Since all calculations are performed in loops for a whole series at once, the threshold had to be adapted to the image in the series showing the darkest vessel, which also can introduce redundant noise in the other images.

The erosion and dilation steps experience similar problems. For all series the structuring element has to be checked and, if necessary, adapted. The same goes for the number of erosion or dilation steps. Too few erode steps can leave behind noise in the selected coordinates, while too many erode steps can make the area of interest fully disappear. For dilation it is the other way around. Just like the threshold, the parameters have to be adapted to the images with least quality, which can introduce inaccuracies in the other images.

Since the threshold, erosion and dilation are done before all the other steps in analysis all further calculations can suffer from the incorrect vessel wall detection. For example when a selection area disappears during erosion, it will not reappear during dilation. No accurate surface calculation can then be done for that series. When too many coordinates are selected as being inside the artery, too large a surface is calculated and the flow will be affected.

Active snake segmentation

The active snake method also has several limitations. A structural error is always introduced with this method in the cross sectional area and the diameter. The minima of the inverse Gaussian derivative image, which we use for detection, lie just outside the vessel (Figure 4.10 and section 4.2.3). For the patient shown in Figure 5.2, we can see that this error in the diameter is of the order 2 mm. For larger vessels the error becomes relatively smaller.

The first error in the segmentation procedure can be introduced by choice of the starting position of the snake. This starting position is defined in one image and used in all images during one heart phase. Due to movement of the vessel, which is observed in endurance athletes, this starting position is not always suitable for all images.

Furthermore the choice of the parameters $\alpha$, $\beta$ and $\gamma$ affects the measurement to a considerable extent. It was determined by trial and error that for this research in most images the best choice of parameters is: $\alpha = 0.35$, $\beta = 0.65$ and $\gamma = 1.5$. When these parameters are slightly changed a small error is introduced in the detected contour. The effects of different values between 0 and 1 have been shown by Panday [31].

Errors in images with low contrtast occur significantly less than with the threshold method. Because of the Gaussian derivative, the image on which the snake operates is blurred and noise or extreme outliers play a less important role. The rigidity and continuity of the snake are provided for with the defined external forces and right choice of parameters. Because of the rigidity of the snake, little problems are experienced from other bright appearing structures in the neighbourhood of the artery of interest in this segmentation technique.

Comparison of methods

If we compare the two methods described above with manual detection for one artery in one image (Figure 5.1), several things can be concluded. As already discussed, we observe that the active shape method results in a overestimation of the area. Both the manual and threshold method show the opposite, a narrow detection. Not all velocity information is inside the detected edge. The manual detection as well as the threshold method is performed to find the edge of a bright appearing structure, the

artery. However at the edge of the artery there is grey shading, which belongs to the artery too and is not accurately detected by these methods. This can introduce errors in the measurement of the diameter and area. At the wall the velocity is low and therefore the error in the velocity and flow measurements will be small.
The detection methods for a whole series of one patient at one location, as shown in Figure 5.2, show no large differences in magnitude and shape, except for the discussed deviation in the cross sectional area and diameter.
From Table 5.1 we can conclude that the active shape method shows the smallest relative variation in the area during systole and therefore is better reproducible. Furthermore the limitations and disadvantages of the threshold method outweigh the limitations of the active shape method. In images, where the arteries are hard to distinguish from the back ground, large mistakes are made with the threshold method. Arteries disappear in the erosion step and cannot be reconstructed. No artery is detected at all and no values can be calculated.
Since manual detection is not an option for analysing large groups of patients, because it is very time consuming, we have chosen active shape as the most suitable method for detection of the arteries in the images of this research. The two main reasons are higher reproducibility and still reasonable results in low contrast images. Because too many pixels in an image are classified as being inside the vessel a small error is introduced in the measured cross sectional area and diameter. It has hardly any influence on the flow or velocity, since the velocity in the additional pixels is zero.
Even though the goal was to (semi)-automatically detect the vessels, both methods still need user interaction. For the threshold method the threshold value, number of erode and dilate steps and the structuring element have to be adapted manually if the vessel was not detected correctly. In the active shape method all interim results were shown and if necessary the starting position of the snake and the parameters $\alpha$, $\beta$ and $\gamma$ could be adapted manually if the snake did not detect the vessel wall correctly.

## 5.2 Volunteer study

The volunteer study in this research has been done for two major purposes:

- To find a measure for the variability between heart beats in velocity, flow and cross sectional area
- To determine the error caused by not perpendicular planning of the MRI images.

Both are interesting for the way of planning MRI scans. The current method, taking the slice as perpendicular as possible to both vessels (further denoted as the MMC-classical method) has the advantage of imaging both vessels and acquiring their cross sectional area and velocity information at exactly the same time and the same heart beat. However since it is almost impossible to choose a slice exactly perpendicular to both vessels due to the human anatomy an error is made in the measured velocity and cross sectional area. Two series were measured exactly perpendicular to the left and the right artery respectively, which will further be referred to as the perpendicular method.

### 5.2.1 Results

Variability between heart beats.
All images of the volunteers were analyzed in the same way as the patient images, resulting in series of numbers for cross sectional area, flow and velocity. The graphs of one volunteer are shown in Figure 5.4. The graph of the cross sectional area shows clearly a large variability, up to 15%, between heart beats (diamonds with different tints) and also a clear difference between the perpendicular series (star in light tint) and the three MMC-classical series. The perpendicular series shows an

almost straight line, since hardly any variation in area during one heart beat was observed, when analysing the artery in a slice exactly perpendicular to this artery.

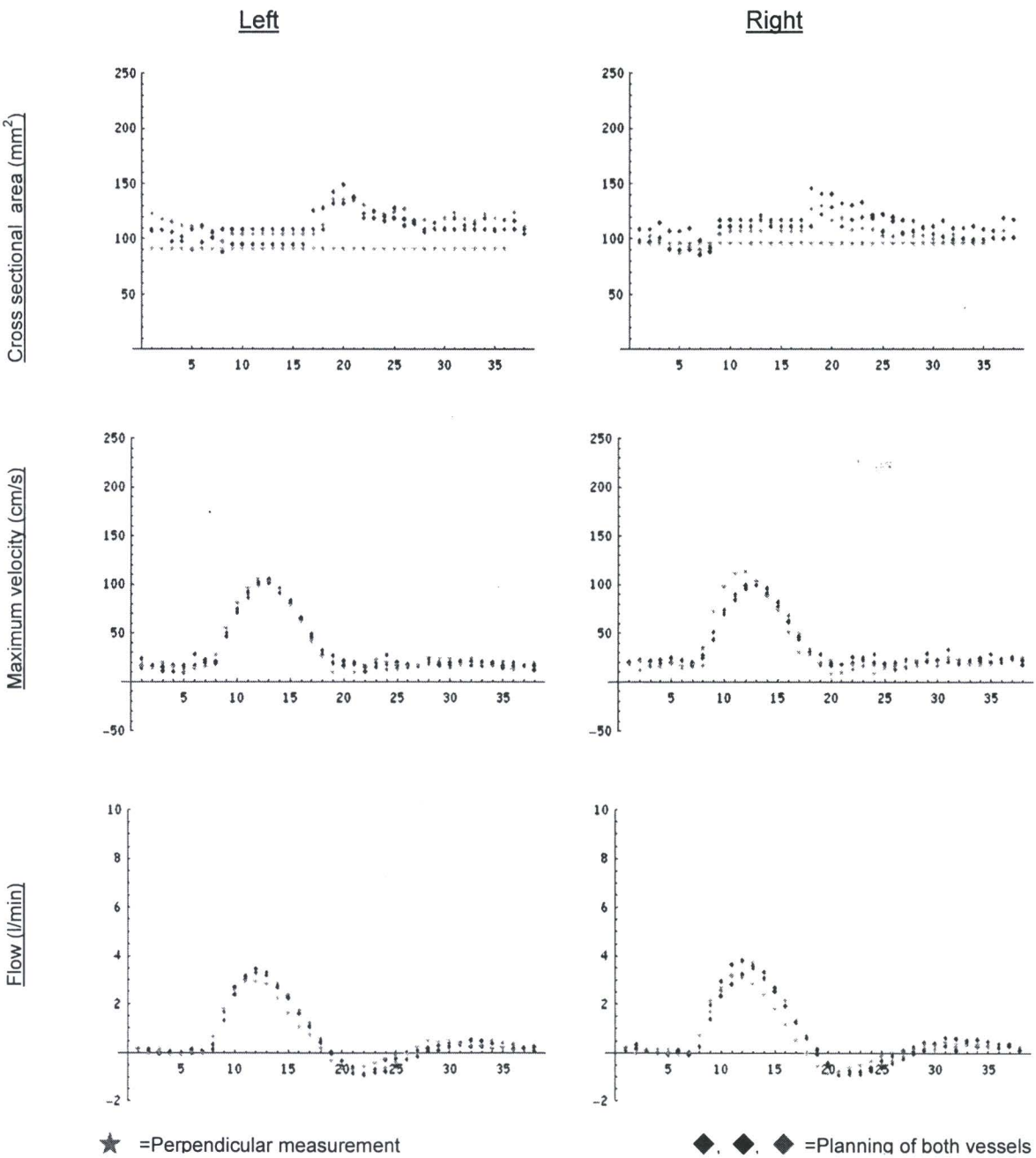


*Figure 5.4: Graphs for volunteer 1*

The variability between heart beats can be calculated by comparing the parameters in the three MMC-classical series image by image. For each image the mean and standard deviation of these three series is calculated. The mean of all standard deviations (as a percentage) over the whole series is a measure for the variability. The exact calculation methods are described in Appendix 3 and the results are shown in Table 5.2.

In Table 5.2 the area shows variations of ~10% and the maximum velocity of ~16%, with a few outliers. The flow shows much larger values for the variation between heart beats. This can be explained by the fact that the flow during diastole is nearly zero and the variation in terms of percentage becomes very large then.

| Volunteer: | | 1 | 2 | 3 | 4 | Average |
|---|---|---|---|---|---|---|
| Area | Left | 5.8 | 13.6 | 11.1 | 9.2 | 9.6% |
| | Right | 6.9 | 11.5 | 10.7 | 8.2 | |
| Flow | Left | 141.4 | 10.0 | 527.4 | 63.0 | 124.3% |
| | Right | 44.5 | 162.7 | 18.1 | 26.9 | |
| Max. Velocity | Left | 12.0 | 20.5 | 13.0 | 16.5 | 16.2% |
| | Right | 13.2 | 17.7 | 14.3 | 22.5 | |

*Table 5.2: Mean of the standard deviations in percentage between the three MMC-classical series.*

Effect of the way of planning the MR images

Since the perpendicular series does not necessarily have the same number of images as the three MMC-classical series we can not calculate the difference image by image. Therefore the values for area, maximum velocity and flow will be compared during systole, for the three pictures with the highest flow. The difference of these parameters between the mean of the three MMC-classical series and the perpendicular series is calculated in percentage. The mean of these percentages in the three pictures during systole is a measure for the effect of misalignment in the planning according to the MMC-classical method. The exact calculation methods are described in Appendix 3.Table 5.3 shows the results.

| Volunteer: | | 1 | 2 | 3 | 4 | \|Average\| |
|---|---|---|---|---|---|---|
| Area | Left | -11.0 | | 1.8 | 24.0 | 13.2% |
| | Right | -6.6 | 12.8 | -17.7 | 18.8 | |
| Flow | Left | -9.5 | | 1.8 | -0.3 | 4.6% |
| | Right | -3.8 | -8.0 | -3.7 | -5.4 | |
| Max. Velocity | Left | 4.2 | | 18.9 | -0.9 | 9.3% |
| | Right | 12.5 | -7.1 | 10.2 | 11.5 | |

*Table 5.3: Mean difference in percentage between the perpendicular series and the mean of the three MMC-classical series.*

Table 5.3 shows similar differences as observed in Table 5.2 for area and maximum velocity. The values for the left leg of volunteer 2 are not available. Remarkable are the large positive area difference between the perpendicular series and the MMC-classical series in volunteer 4.

Arterial Stiffness

With the blood pressure measurement at the end of the volunteer examination, we can estimate the distensibility and compliance coefficient of the external iliac arteries of the volunteer as described in section 2.3, Formula 2.14 and 2.15.

Both A and $\Delta A$ were taken from the mean of the three MMC-classical series. Table 5.4 shows the parameters A, $\Delta A$, $\Delta P$ and the calculated compliance coefficient (CC) and distensibility coefficient (DC). Area is expressed in $mm^2$ and pressure in mmHg and kPa. mmHg is the standard unit for measuring blood pressure, but to be able to compare the results we need CC and DC in units of $mm^2/kPa$ and $kPa^{-1}$ respectively.

| | | $\Delta P$ (mmHg) | $\Delta P$ (kPa) | $\Delta A$ ($mm^2$) | A ($mm^2$) | CC ($mm^2/kPa$) | DC ($kPa^{-1}$) |
|---|---|---|---|---|---|---|---|
| Volunteer 1 | Left | 71 | 9.443 | 40.3 | 113.5 | 4.29 | $37.6 \cdot 10^{-3}$ |
| | Right | 75 | 9.975 | 39.5 | 105.0 | 3.99 | $37.6 \cdot 10^{-3}$ |
| Volunteer 2 | Left | 55 | 7.315 | 20.3 | 85.5 | 2.78 | $32.3 \cdot 10^{-3}$ |
| | Right | 61 | 8.113 | 27.2 | 88.8 | 3.38 | $37.6 \cdot 10^{-3}$ |
| Volunteer 3 | Left | 56 | 7.448 | 43.7 | 136.8 | 5.87 | $42.9 \cdot 10^{-3}$ |
| | Right | 60.5 | 8.047 | 59.2 | 162.2 | 7.37 | $45.1 \cdot 10^{-3}$ |
| Volunteer 4 | Left | 73 | 9.709 | 47.7 | 105.7 | 6.39 | $60.9 \cdot 10^{-3}$ |
| | Right | 78.5 | 10.441 | 36.7 | 99.0 | 4.59 | $45.9 \cdot 10^{-3}$ |

*Table 5.4: Results of distensibility and compliance calculations for volunteers*

Remarkable in Table 5.4 was the large variation in CC and DC between volunteers. Furthermore all volunteers showed differences in Compliance between their left and right leg. 3 out of 4 volunteers showed a difference in distensibility between the left and right leg. The largest differences between left and right for all parameters in Table 5.4 were found in volunteer 4.

### 5.2.2 Discussion

Variability between heart beats.

To start with the variability between heart beats, it is relatively large as can be concluded from Table 5.2. Variations of ~10% are seen in the area and ~16% in the maximum velocity. From the large values in the variation of the flow no conclusions can be drawn, since they are caused by the nearly zero flow during diastole.

Effect of the way of planning the MR images

During systole when the velocity is largest, the largest difference is expected due to misalignment. In Table 5.3 we observe that the difference between the perpendicular image series and the MMC-classical series in percentage is of the same order as the variability between heart beats. The area shows a slightly higher variation (~13%), while the maximum velocity shows a lower value (~9%). From this result we can state that the error due to misalignment in the MMC-classical method does not weigh up against the opportunity to measure both vessels at the same time during the same heart beat. Furthermore the flow only shows little variation (~5%) as can be expected since the same blood passes through the vessel, independent of the cross section we look at.

For the perpendicular series we expect smaller area and larger velocity than the MMC-classical series. Therefore we would expect predominantly negative values for the area and positive values for the maximum velocity in Table 5.3, but this is not observed. Most differences observed, both positive and negative are within the range of variability between heart beats. Volunteer 4 however shows a larger area in the perpendicular than in the MMC-classical series, outside the calculated variability between heart beats. This may be a result of the asymmetry in his iliac arteries, which made the planning of the perpendicular images very difficult.

Arterial Stiffness

Little literature is available concerning compliance and distensibility coefficient in endurance athletes. Bortel et al. [23] shows that in the systemic arteries in healthy volunteers values between $28 \cdot 10^{-3}$ and $32 \cdot 10^{-3}$ $kPa^{-1}$ are measured for the distensibility coefficient. Our volunteers show values between $32 \cdot 10^{-3}$ and $45 \cdot 10^{-3}$ $kPa^{-1}$, with one peak to $60 \cdot 10^{-3}$ $kPa^{-1}$. These large values in our study for the distensibility coefficient could have several causes: Overestimation of the cross sectional area by our active shape segmentation method or underestimation of the blood pressure. Bortel also had very strict inclusion criteria for the volunteers in his study in order to exclude confounding factors that could have influence on the blood pressure in this measurement, e.g. no smoking and no beverages containing caffeine. These inclusion criteria were not applied to the volunteers in our study and this certainly had influence on the results of our measurements. Further investigation on this subject is needed to be able to state if these coefficients are suitable for recognising vascular problems in endurance athletes

## 5.3 Retrospective study on MRA images

All patients in our study group suffered from kinking and intravascular damage, resulting in a stenosis in the left external iliac artery. The exact location is not known during MR planning but the quantitative flow images were made in or very close to the stenosis. In the images of both the patients and the controls the vessels were

detected by active shape segmentation and the parameters of interest were calculated as described in section 4.3.

### 5.3.1 Results

All three locations were analysed: 2 cm below aorta bifurcation, 2 cm below iliac bifurcation and 2 cm above femoral bifurcation, denoted as Common, External and Femoral respectively. The results are from the images acquired with stretched legs, since the images made with flexed hips did not always show the arteries of interests or the slices were taken in a curvature of the artery and were therefore hard to analyse. The investigated parameters were cross sectional area, diameter, (peak) flow and peak systolic velocity. The diameter will not be further discussed, because it is directly related to cross sectional area and shows similar results. The differences in the parameters between the left and right leg during systole (in percentage) were calculated by the methods described in Appendix 4. Figures 5.5 a and b show the results for peak systolic area and velocity, respectively.

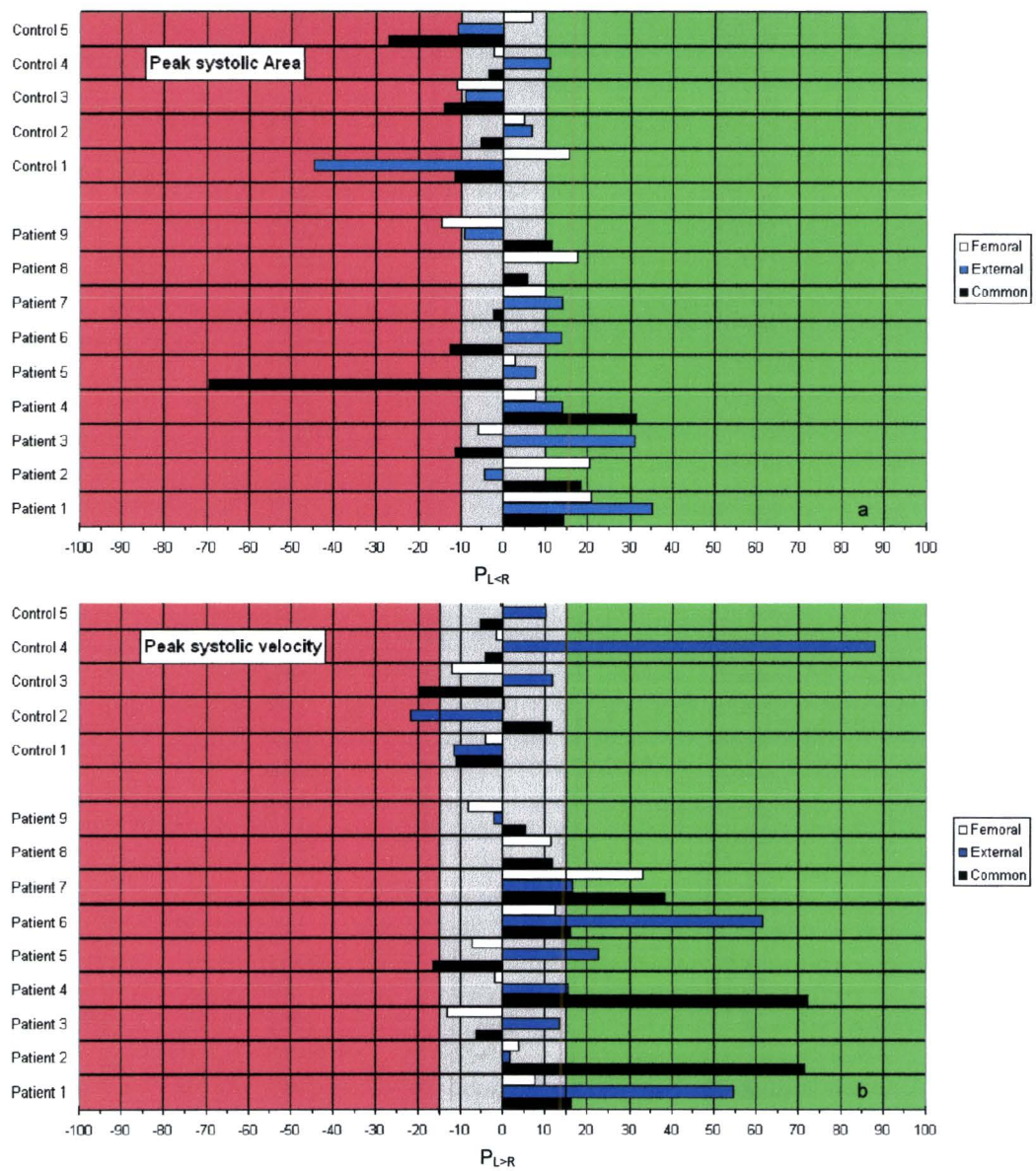


*Figure 5.5: Differences between left and right in terms of percentage for the peak systolic area (a) and velocity (b).*

In these graphs the horizontal axes denotes the differences between Left (L) and right (R) in terms of percentage. For the area we use the percentage L<R with respect to R, denoted as $P_{L<R}$ and for the maximum velocity the percentage L>R with respect to R, denoted as $P_{L>R}$. The light grey area denotes the area were the differences between left and right are not significant (<10% for area and <15% for velocity). These significance boundaries are chosen on basis of the outcome of the volunteer study on variation between heart beats. The green area denotes a significant difference between left and right: (R-L)/R>10% for the area and (L-R)/R>15% for the velocity. The red area denotes a significant difference in the opposite direction. Appendix 5 shows a table with the calculated numbers and the same colour indication as the graphs of Figure 5.5.
In Figure 5.5 we see that 5 out of 8 patients show significant smaller values for left compared to right for the area and significantly larger values for left compared to right for the maximum velocity at the external iliac arteries. Significant differences are also seen at other locations of the patients:

- 4 out of 9 in both the common iliac artery and femoral artery show significant smaller area left compared to right.
- 5 out of 9 in the common iliac artery and 1 out of 9 in the femoral artery show significant larger velocity left compared to right.
- 3 out of 9 in the common iliac artery and 1 out of 9 in the femoral artery show significant larger area left compared to right.
- 1 out of 9 in the common shows significant smaller velocity left compared to right.

Significant differences in both directions for all three locations are also observed in the controls, a total of 12 out of 30 measurements.
Appendix 6 shows the graphs for the area, flow and maximum velocity in the external iliac arteries of the patients. The large differences as seen in Figure 5.5 can also be observed in the graphs in Appendix 6. Images of the external iliac artery of patient 8 were not available and therefore no results could be calculated.

### 5.3.2 Discussion

Due to the stenosis in the external iliac artery of the patients we expect the velocity to be higher in the left leg than in the right leg at the location of the stenosis. For the injured artery a decrease in elasticity is expected, which means that the cross sectional area and diameter are expected to be higher in the healthy (right) artery, especially during systole.
The results presented in the previous section show the expected result for the iliac artery in 5 out of 8 patients: Patient 1, 4, 5, 6 and 7 show significant (>10%) smaller area in the external iliac artery and Patient 1, 3, 4, 6 and 7 show significant (>15%) velocity in the external iliac arteries. In literature [5] research on the relation between area decrease and velocity increase was described on basis of observations with Echo-Doppler. For stenosis up to 20% reduction of lumen diameter (~36% reduction in lumen cross sectional area) only subtle changes in the velocity could be measured. Stenosis occupying 20-49% of the lumen diameter showed a 30-100% increase in peak systolic velocity. The decrease in area in the stenosed arteries in our study group was less then 36% in all patients as can be seen from Figure 5.5, which corresponds to a decrease in lumen diameter less than 20%, in comparison to the healthy leg. Still we could measure increase in peak systolic velocity up to 61%. This suggests that with this method even slightly stenosed arteries can show significant differences in the area and velocity in comparison to healthy vessels. However in 3 out of 8 patients with stenosed external iliac arteries no significant differences were found in area or velocity. From this it seems that the method of quantitative flow imaging and the analysis as described in this report is not very sensitive.
In the common and femoral artery no obvious pattern can be seen. Because the stenosis is in the external iliac artery, no significant differences between left and right

are expected in these arteries. However 7 out of 9 patients show significant differences between left and right in the common iliac artery in both directions in the area (4/9 L<R and 3/9 L>R). Significant differences for velocity in the common are observed in 6 out of 9 patients (5/9 L>R and 1/9 L<R). In literature, studies were found on the asymmetry and non-planarity of the aorta bifurcation in humans [33], which could cause these differences. This asymmetry and non-planarity were measured with MR methods and showed large variations of branching and toroidally curvatures out of plane of both iliac arteries, but more common on the right side.
The femoral artery does not show many significant differences between left and right. For velocity only 1 out of 9 showed a difference larger than 15% (L>R). For the area 4 out of 9 patients showed significant differences between left and right in the femoral artery (3/9 L<R and 1/9 L>R). To our best knowledge no previous research has been done on naturally occurring asymmetry in the femoral arteries. No values were available to compare our results with. There is a chance that some of the differences measured in the femoral artery are still an effect of the stenosis in the external iliac artery. The images we denote as femoral were made just above the femoral bifurcation, close to the external iliac artery.
For the controls, endurance athletes with no history of vascular problems, no significant differences between left and right were expected either. From Figure 5.5 however we do see differences. In the common iliac artery 3 out of 5 controls showed significant difference in the area (L>R) and 1 out of 5 controls for the velocity (L<R). This could be a result of the earlier mentioned asymmetry of the aorta bifurcation in humans [33]. In the external iliac artery 3 controls showed significant differences in the area (2/5 L>R and 1/5 L<R) and 2 controls in the peak systolic velocity (1/5 L<R and 1/5 L>R). Finally in the femoral artery only significant differences were found in the area, of two controls (1/5 L<R and 1/5 L>R). For these differences in the external iliac artery and the femoral artery no plain explanation can be given. No values from literature are available to compare the results to and we have to interpret it as natural human asymmetry. Due to this asymmetry our method of quantitative flow imaging and analysis appears to show a low specificity.
In the diameters and velocity measured with Echo-Doppler (section 1.4) in the common and the external iliac artery (*proximal* and distal tot the stenosis) of our patients similar asymmetry is observed, no clear differences between left and right in one direction. This suggests that our measurement method is accurate, but indeed has a low specificity due to natural human asymmetry
The stenosed arteries was expected to be less elastic, however arterial stiffness calculations as performed in the volunteer study were not possible, since no values for $\Delta P$ were available. As described in section 1.4 blood pressure measurements were done during exercise. From these measurements only the ankle-arm indices were available for all patients in our study group. The values of this index was significant larger in the right leg than in the left leg for all patients, but from these results it is not allowed to assume a larger pressure in the right leg compared to the left leg.
The reliability of the described method depends for a great deal on the accurateness of the segmentation method. If the artery of interest is not detected accurately, too much or too little information is taken into account and errors are introduced in the calculated parameters. In this research user interaction was required during the segmentation and for all detected arteries the resulting snake was visually checked. Therefore we expect small errors due to the segmentation technique, but the user interaction lowers the reproducibility.
Another limitation of the method described in this research is the imaging technique. The exact location of the imaged slices was not known, but it was chosen in the stenosis, if visible. Images that were not made exactly in the stenosis can result in measurements of unexpected values in area and velocity. Furthermore we image just one slice and measure the velocity only perpendicular to that slice. Secondary

velocity profiles, which could influence the flow and the impression of the velocity profile, cannot be measured. For curved arteries, as they occur in endurance athletes, the planning of the slice is difficult.
In this retrospective study the MMC-classical method (Section 4.1.2) was used, both arteries were measured as perpendicular as possible in one slice and on that accounts no error was introduced due to variability between heart beats. On the other hand with the MMC-classical an error method could be introduced due to misalignment. From the volunteer study we learned this is not a large error (~13% in area and ~9% in maximum velocity).

# 6 Conclusion and recommendations

The purpose of this study was to investigate whether vascular problems in endurance athletes can be detected using MRI and in particular a QF technique. Different segmentation techniques were used for vessel detection. Manual detection was not suitable for analysing larger groups of patients, because it was very time consuming. Two possible alternatives were the threshold method and active shape segmentation, which were both developed and tested in this research. Active shape segmentation had a high reproducibility and it experienced little difficulties with low contrast images where the vessels were hard to distinguish from the background or with images where other bright structures appear close to the vessel of interest. However a small error was always introduced in the detected area. The threshold method on the other hand had much more difficulties with low contrast images. If the vessel was hard to distinguish from the background, it disappeared during the erosion step and no vessel was detected at all. Other bright structures close to the vessel of interest were detected with the threshold too and did not always disappear during erosion, resulting in a detected area much larger than the vessel of interest. Weighing these advantages and disadvantages, active shape segmentation was chosen as the preferred method for vessel detection in this research.
Following segmentation the velocity information in the arteries of interest was extracted and the diameter and cross sectional area of the arteries were calculated.

From a volunteer study we concluded that the error introduced by selecting a slice not exactly perpendicular to the arteries, in imaging both arteries at the same time is of the same magnitude as the variability between heart beats, for all investigated parameters.

The patient group in the retrospective study consisted of endurance athletes all suffering from serious vascular problems in the left external artery. Due to large inter-human variability the best comparison could be made in one patient between the healthy and the stenosed external iliac artery. Most patients showed a clear difference between the stenosed and the healthy artery. Even slightly stenosed arteries showed decreased cross sectional area and increased peak systolic velocity, although not all patients with a stenosis showed clear differences between the left and right leg and the described method appeared to have a low sensitivity.
A large variation in the evaluated parameters between the left and the right leg in controls and at non-affected regions of patients was observed too. This made the quantitative flow images and the described analysis technique unsuitable for individual diagnosis, because it appears not to be specific.

Further research is needed to investigate whether new techniques could improve the examinations. We advise a further exploration of 3D PCA. Using quantitative flow information in the whole stenosed part of the artery instead of one slice is likely to give more information concerning the vascular problem. Another interesting subject for further investigation are the coefficients for arterial stiffness. More accurate measurement of the local blood pressure is needed for reliable calculation of these coefficients.

## Literature


[1] CHEVALIER JM, ENON B, WALDER J, BARRAL X, PILLET J, MEGRET A, LHOST SAINT-ANDRE JP, DAVINROY M. *Endofibrosis of the external iliac artery in bycicle racers: an unrecognized pathological state.* Ann Vasc Surg. 1986 Nov; 1 (3): 297-303.

[2] BENDER MHM, SCHEP G, VRIES WR DE, HOOGEVEEN AR, WIJN PFF. *Sports-Related Flow Limitations in the Iliac Arteries in Endurance athletes.* Sports Med. 2004, Approval for publication.

[3] KLERKX G. *De inspanningstest als diagnostisch instrument voor inspanningsgerelateerde iliacale vaatproblematiek bij duursporters.* 2003 Nov. Graduation thesis, University Maastricht.

[4] AGUR AMR. *Grant's Atlas of anatomy.* 1991 Ninth edition, Williams & Wilkins, Baltimore

[5] SCHEP G. *Functional vascular problems in the iliac arteries in endurance athletes.* 2001 Thesis, University of Utrecht

[6] COYLE EF, FELTNER ME, KAUTZ SA, HAMILTON MT, MOUNTAIN SJ, BAYLOR AM, ABRAHAM LD, PETREK GW. *Physiological and biomechanical factors associated with elite endurance cycling performance.* Med Sci Sports Exerc. 1991 Jan; 23 (1): 93-107

[7] SCHEP G, BENDER MHM, KAANDORP D, HAMMACHER E, VRIES DWR. *Flow limitations in the iliac arteries in endurance athletes: current knowledge and directions for the future.* Int J Sports Med. 1999; 20: 421 – 428

[8] CHEVALIER JM, ENON B, WALDER J, BARRAL X, PILLET JM, L'HOSTE PH, ET AL. *Endofibrosis of the external iliac arteryin bicycle racers : an unrecognized pathological state.* Ann Vasc Surg. 1986 Nov; 1 (3): 297 – 303

[9] ROUSSELET MC, SAINT-ANDRE JP, L'HOSTE P, ENON B, MEGRET A, CHEVALIER JM. *Stenotic intimal thickening of the external iliac artery in competition cyclists.* Human Pathol. 1990 May; 21 (5): 524 – 529

[10] MCDONALD DA. *Blood flow in arteries.* 1974, Edward Arnold (Publishers) Ltd. London

[11] VOSSE FN VAN DE, DONGEN MEH VAN. *Cardio Vascular Fluid mechanics.* 1998, lecture notes. Eindhoven University of Technology

[12] PARKER KH, CARO CG. *Flow in the macrocirculation: basic concepts from fluid mechanics.* Chapter 6: POTCHEN EJ, et al.: *Magnetic Resonance Angiography.* 1993, Mosby-Year Book, Inc. St Louis

[13] DEAN WR. *The stream-line motion of fluid in a curved pipe.* Philos Mag. 1928; 5: 673

[14] MILNOR WR. *Hemodynamics.* 1989, Williams & Wilkins. Maryland

[15] PALMEN DEM, VOSSE FN VAN DE, JANSSEN JD, DONGEN MEH VAN. *Analysis of the flow in stenosed carotid artery bifurcation models – hydrogen bubble visualisation.* J Biomech, 1994; 27 (5): 581-590.

[16] YOUNIS HF, KAAZEMPUR-MOFRAD MR, CHAN RC, ISASI AG, HINTON DP, CHAU AH, KIM LA, KAMM RD. *Hemodynamics and wall mechanics in human carotid bifurcation and its consequences for atherogenesis: investigation of inter-individual variation.* Biomech Model Mechanobiol. 2004 Sep;3(1):17-32.

[17] PEDLEY TJ. *The fluid mechanics of large blood vessels.* 1980, Cambridge University Press

[18] WOMERSLEY JR. *Oscillatory flow in arteries: effect of radial variation in viscosity on rate of flow.* J Physiol. 1955 Feb 28;127(2):38-39.

[19] GIJSEN FJH, ALLANIC E, VOSSE FN VAN DE, JANSSEN JD. *The influence of the non-Newtonian properties of blood on the flow in large arteries: unsteady flow in a 90° curved tube.* J Biomech, 1999; 32: 705-713.

[20] VOSSE FN VAN DE, HART J DE, OIJEN CHGA VAN, BESSEMS D, GUNTHER TWM, SEGAL A, WOLTERS BJBM, STIJNEN JMA, BAAIJENS FPT. *Finite-element-based computational methods for cardiovascular fluid-structure interaction.* J Eng Mathem, 2003; 47: 335-368.

[21] OYRE S, PEDERSEN EM, RINGGAARD S, BOESIGER P, PAASKE WP. *In vivo Wall Shear measured by magnetic resonance velocity maping in the normal human abdominal aorta.* Eur J Vasc Endovasc Surg. 1997 Mar;13(3):263-271

[22] SHAABAN AM, DUERINCKX AJ. *Wall Shear Stress and Early Atherosclerosis.* Am J Roentgenol. 2000 Jun; 174 (6):1675-1665

[23] BORTEL LM V, DUPREZ D, STARMANS-KOOL MJ, SAFAR ME, GIANNATTASIO C, COCKCROFT J, KAISER DR, THUILLEZ, C. *Clinical applications of arterial stiffness, task force III: Recommendations for user procedures.* Am J Hypertension, 2002 May; 15 (5): 445-452.

[24] VLAARDINGERBROEK MT, BOER JA DEN. *Magnetic Resonance Imaging, theory and practice.* 1999 Springer-Verlag, Berlin

[25] HORNAK JP. *The basics of MRI.* Http://www.cis.rit.edu/htbooks/mri, 2000 CD-rom

[26] HASHEMI RH, BRADLEY WG. *MRI the basics.* 1997 Williams & Wilkins, Baltimore.

[27] GONZALEZ RC, WOODS RE. *Digital Image processing.* 1992, Addison-Wesley Publishing Company, Inc. USA

[28] HAAR ROMENY BM TER. *Front-End Vision and Multi-Scale Image Analysis: Multi-Scale Computer Vision Theory and Applications, written in Mathematica.* 2003, Kluwer Academic Publishers, Dordrecht

[29] http://www.itk.org/HTML/GaussianFilter.htm

[30] KASS M, WITKIN A, TERZOPOULOS D. *Snakes: Active contour models.* Intern J Comput Vis, 1988; 1 (4):321-331.

[31] PANDAY V. *Segmentation techniques for the visible mouse.* 2003 June. Graduation thesis, Eindhoven University of Technology.

[32] WEISSTEIN EW. *http://mathworld.wolfram.com.*

[33] XU XY, LONG Q, BOURNE M, GRIFFITH TM. *On the geometrical and flow characteristics of the human abdominal aorta.* 1999 June, Bioengineering conference, Montana.

[34] WIJN PFF, SAR P VAN DER, GOOTZEN THJM, TILMANS MHJ, SKOTNICKI SH. *Value of the spectral broadening index in continuous wave Doppler measurements.* Med & Biol. Eng & Comput, 1987; 25(4): 377-385.

# Appendix 1 Terminology list

In this list the italic printed words in this report are translated and/or explained in Dutch

| | |
|---|---|
| *Adhesion* | Verkleving |
| *Aetiology* | De leer der ziekte-oorzaken |
| *Atherosclerosis* | Aderverkalking |
| *CFD* | Computational Fluid Dynamics, de tak van wetenschap die zich bezighoudt met het kwantitatief voorspellen van (complexe) vloeistofstroming |
| *Claudication* | Afsluiting van arteriën, welke ischemie van de beenspieren veroorzaakt |
| *Coccyx* | Stuitbeentje |
| *Compliance* | Compliantie, rekbaarheid |
| *Distal* | Het verst van de oorsprong, in dit geval van het hart |
| *Distensibility* | Distensibiliteit, uitzetting |
| *Groin* | Lies |
| *Hermite polynomials* | Hermite polynomen ($H_n(x)$) is een set van orthogonale polynomen over het domein (-∞,∞). De eerste 5 Hermite polynomen zijn [32]: $H_0(x)=1$, $H_1(x)=2x$, $H_2(x)=4x^2-2$, $H_3(x)=8x^3-12x$, $H_4(x)=16x^4-48x^2+12$ (A1.1) |
| *Hypertrophy* | Sterke ontwikkeling van weefsels of organen (in dit geval spier) |
| *In vitro* | Buiten het lichaam |
| *In vivo* | In het lichaam zelf |
| *Lesion* | Beschadiging |
| *Laplacian* | Laplace operator. De 2D Laplace operatoor in Cartesische coördinaten word gegeven door [32]: $\Delta\phi = \frac{\partial^2\phi}{\partial x^2} + \frac{\partial^2\phi}{\partial y^2}$ (A1.2) |
| *Lumbar vertebra* | Lende wervel |
| *Non-invasive* | Niet inwendig, er hoeven geen instrumenten de huid te passeren |
| *Polygon* | Een gesloten vlakke figuur, opgebouwd uit verschillende lijn segmenten die verbonden zijn. |
| *Proximaal* | Het dichts bij de oorsprong, in dit geval het hart |
| *Psoas muscle* | Psoas spier, belangrijkste spier bij heupflexie |
| *Spinal column* | Wervelkolom |
| *Stenosis* | Stenose, vernauwing |
| *Systole* | Samentrekking van de hartkamers |
| *Unilateral* | Éénzijdig |
| *Ventral* | Ventraal, aan de buikzijde |

# Appendix 2 Plug flow

When the bifurcations and curvatures, leading to complex flow profiles, are not taken into account a plug flow can be assumed in arteries. The general formula for plug flow is [34]:

$$v(r) = v_{max}\left(1 - \left(\frac{r}{R}\right)^{k}\right), \tag{A2.1}$$

with $v$ the velocity, $v_{max}$ the maximum velocity, $R$ the radius of the vessel, $r$ the distance form the centre of the vessel ($r \leq R$) and $k$ a constant that can be calculated by:

$$v_{mean} = \left(\frac{k}{k+2}\right)v_{\max}, \tag{A2.2}$$

with $v_{mean}$ the mean velocity over the artery.

If we take values for $v_{max}$ and $v_{mean}$ as measured in a patient:

$v_{max}$ = 130.5 cm/s

$v_{mean}$ = 88.0 cm/s

We can calculate k by formula A2.2, resulting in:

$k$ = 4.15

The plug flow according to formula A2.1 is shown Figure A2.1

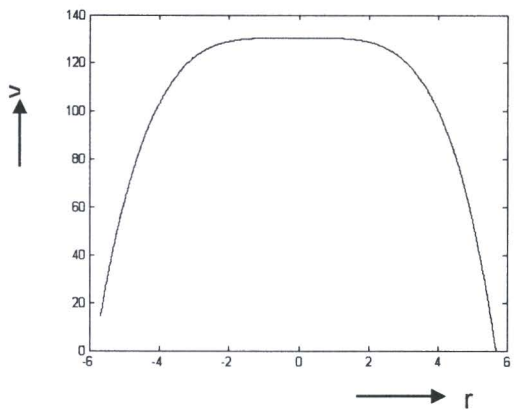


*Figure A2.1: Expected plug flow in an artery*

Figure A2.1 shows that the velocity profile is practically flat within a radius of 2 mm. The area corresponding to a radius of 2 mm is:

$$a_{flat} = \pi \cdot r^2 = \pi \cdot 2^2 = 12.6mm^2$$

Since the pixels of the images in this research have an area of 1 mm$^2$, the velocity profile is flat within a radius of at least 12 pixels. If the mean of 10 pixels with the highest value is taken to calculate the maximum velocity, this is justified.

# Appendix 3 Calculation methods volunteer study

Like for the retrospective study also for the volunteer study some recapitulating numbers are needed. We are interested in the variation between heart beats and the difference between the slice selection exactly perpendicular to one artery or as perpendicular as possible to both arteries.

## A3.1 Variation between heart beats

The variation in the parameters between heart beats is calculated from the three equally acquired image series. These series all have the same length and the comparison can be made image by image. The method is the same for all three parameters of interest; area, flow and maximum velocity, the general procedure will be described here. We can define the three series of one parameter for left and right by:

Measurements left: $\boldsymbol{a_1} = (a_{11}, a_{12}, \ldots, a_{1n})$, $\boldsymbol{a_2} = (a_{21}, a_{22}, \ldots, a_{2n})$ and $\boldsymbol{a_3} = (a_{31}, a_{32}, \ldots, a_{3n})$

Measurements right: $\boldsymbol{b_1} = (b_{11}, b_{12}, \ldots, b_{1n})$, $\boldsymbol{b_2} = (b_{21}, b_{22}, \ldots, b_{2n})$ and $\boldsymbol{b_3} = (b_{31}, b_{32}, \ldots, b_{3n})$

For each image we can calculate the mean and standard deviation of the three series according to:

Mean:

$$\bar{\boldsymbol{a}}_i = \frac{\boldsymbol{a}_{1i} + \boldsymbol{a}_{2i} + \boldsymbol{a}_{3i}}{3} \tag{A3.1}$$

Standard deviation:

$$\sigma_{a_i} = \sqrt{\frac{1}{3-1}\sum_{m=1}^{3}\left(\boldsymbol{a}_{mi} - \bar{\boldsymbol{a}}_i\right)^2} \tag{A3.2}$$

This standard deviation gives an absolute deviation of the mean. In terms of percentage it becomes:

$$\sigma_{a_i}^{\%} = \left(\sigma_{a_i} / \bar{\boldsymbol{a}}_i\right) \cdot 100\% \tag{A3.3}$$

The mean of these standard deviations is a measure for the variability between heart beats and is calculated according to:

$$\overline{\sigma_{a_i}^{\%}} = \frac{1}{n}\sum_{i=1}^{n}\sigma_{a_i}^{\%} \tag{A3.4}$$

## A3.2 Effect of misalignment

If the exact perpendicular series had the same number of images as the three equally acquired series the calculation of the effect of misalignment could be done by the method described in the previous section. However the number of images in the exact perpendicular series is of the volunteers mostly smaller. Therefore the best option is to take in both series the three images where the flow is highest, systole, and compare these.

If we take the measurements for flow of one leg we can define the following notation:

Mean of the measurements of the three series: $\boldsymbol{a} = (\bar{a}_1, \bar{a}_2, \ldots, \bar{a}_n)$

Measurements perpendicular: $\boldsymbol{b} = (b_1, b_2, \ldots, b_n)$

From these series we take the 3 highest values and create new series:

3 highest values of $\boldsymbol{a}$: $\boldsymbol{a}_{\max} = (\bar{a}_{m1}, \bar{a}_{m2}, \bar{a}_{m3})$

3 highest values of $\boldsymbol{b}$: $\boldsymbol{b}_{\max} = (b_{m1}, b_{m2}, b_{m3})$

The difference series is then defined as: $\boldsymbol{v} = \boldsymbol{b}_{max} - \boldsymbol{a}_{max} = (b_{m1} - \bar{a}_{m1}, b_{m2} - \bar{a}_{m2}, b_{m3} - \bar{a}_{m3})$

Since we are interested in differences in terms of percentage, we have to dfine a difference series according to:

$$\boldsymbol{v}^{\%} = \left(\frac{v_1}{a_1}, \frac{v_2}{a_2}, \frac{v_3}{a_3}\right) \cdot 100\% \tag{A3.5}$$

If we calculate the mean of this series we will have a number for the error due to misalignment in terms of a percentage. The same can be done for the velocity and area, taking the same three images with maximum flow.

# Appendix 4 Calculation methods retrospective study

To be able to draw conclusions from the measurement results of the retrospective study, some recapitulating numbers are needed, in this case a number for the difference between left and right. This difference can be expressed as a percentage by which the parameter on one side is larger than the parameter on the other side. Since the largest differences can be seen during systole we will calculate the difference in the three pictures in the heart phase were the flow is largest.

## A4.1 Peak flow

If we take the measurements of one series we can define the following notation:
Measurements left: $\boldsymbol{a}=(a_1, a_2, \ldots, a_n)$
Measurements right: $\boldsymbol{b}=(b_1, b_2, \ldots, b_n)$
From these series we take the 3 highest values and create new series:
3 highest values left: $\boldsymbol{a}_{max}=(a_{m1}, a_{m2}, a_{m3})$
3 highest values right: $\boldsymbol{b}_{max}=(b_{m1}, b_{m2}, b_{m3})$
The mean of these series can be calculated according to:

$$\bar{a}_{max} = \frac{a_{m1} + a_{m2} + a_{m3}}{3} \qquad \text{(A3.1)}$$

and:

$$\bar{b}_{max} = \frac{b_{m1} + b_{m2} + b_{m3}}{3} \qquad \text{(A3.2)}$$

Since the flow shows a lot of variation during the systole and is relatively constant during the remaining time of a heart beat (Figure 4.13 d), the systole is the interesting part to compare left and right. For the peak systolic flow the difference between left and right is expressed in a percentage by which left is smaller than right ($P_{L<R}$):

$$P_{L<R} = \left( \frac{\bar{b}_{max} - \bar{a}_{max}}{\bar{b}_{max}} \right) \cdot 100\% \qquad \text{(A3.3)}$$

## A4.2 Cross sectional area

For the cross sectional area we define the measurement series as in the previous section. From these series we take the values at the location were flow was largest. On these values Formulas A3.1 – A3.3 are applied again, resulting in a percentage by which the peak systolic area on the left is smaller than on the right.

## A3.3 Peak systolic velocity

Like the flow and the area, the interesting part of the maximum velocity to compare left and right is during the systole. The definitions of the series and calculations of the mean are similar to the one for peak flow and area (Formulas A3.1 and A3.2). The difference is that we expect the velocity to be larger in the left (injured) artery. For this reason the difference between left and right is expressed as a percentage by which left is larger than right ($P_{L>R}$) and equation A3.3 becomes:

$$P_{L>R} = \left( \frac{\bar{a}_{max} - \bar{b}_{max}}{\bar{b}_{max}} \right) \cdot 100\% \qquad \text{(A3.5)}$$

## A4.4 Variation during diastole

Another interesting number is the variation of cross sectional area during diastole. We expect not much change since velocity and flow are low during the last stage of the heart phase (the diastole).
The series of measurement are defined again as in section A3.1:
Measurements left: $\boldsymbol{a}= (a_1, a_2, \ldots, a_n)$
Measurements right: $\boldsymbol{b}= (b_1, b_2, \ldots, b_n)$
Now we define new series of the measurements during diastole:
Diastole measurements left: $\boldsymbol{a}_{\text{dias}}=(a_i, a_{i+1}, \quad, a_n)$
Diastole measurements right: $\boldsymbol{b}_{\text{dias}}=(b_i, b_{i+1}, \quad, b_n)$
The value i is calculated by: i=[n/4], with the square brackets denoting the nearest integer value. Again we can calculate the mean and variance by:
Mean:

$$\overline{a_{dias}} = \frac{1}{n-i}\sum_{j=i}^{n} a_j \tag{A3.7}$$

Standard deviation:

$$\sigma_{a_{dias}} = \sqrt{\frac{1}{n-i-1}\sum_{j=i}^{n}\left(a_j - \overline{a_{dias}}\right)^2} \tag{A3.8}$$

Likewise for series $\boldsymbol{b}_{\text{dias}}$

## Appendix 5 Table of results of the retrospective study

| | Common | | | External | | | Femoral | | |
|---|---|---|---|---|---|---|---|---|---|
| | Peak Area | Peak Flow | Peak velocity | Peak Area | Peak Flow | Peak velocity | Peak Area | Peak Flow | Peak velocity |
| | %L<R | %L<R | %L>R | %L<R | %L<R | %L>R | %L<R | %L<R | %L>R |
| Patient 1 | 14.40 | -3.70 | 16.43 | 35.31 | 18.22 | 54.68 | 20.94 | 14.31 | 7.59 |
| Patient 2 | 18.41 | -43.80 | 71.45 | -4.35 | 6.73 | 1.83 | 20.34 | 6.45 | 3.90 |
| Patient 3 | -11.34 | 2.37 | -6.15 | 31.12 | 14.88 | 13.41 | -5.86 | 8.31 | -12.95 |
| Patient 4 | 31.35 | -43.91 | 72.16 | 13.93 | 18.07 | 15.59 | 7.65 | 6.32 | -1.68 |
| Patient 5 | -69.48 | 8.52 | -16.22 | 7.73 | 6.41 | 22.58 | 2.70 | 5.62 | -7.02 |
| Patient 6 | -12.54 | 10.29 | 16.17 | 13.73 | -5.22 | 61.53 | -0.56 | 4.23 | 12.44 |
| Patient 7 | -2.19 | -8.30 | 38.15 | 13.94 | 9.29 | 16.70 | 10.00 | 3.38 | 33.14 |
| Patient 8 | 5.69 | -0.24 | 11.70 | | | | 17.71 | 29.39 | 11.59 |
| Patient 9 | 11.59 | 25.32 | 5.30 | -9.12 | 6.39 | -2.16 | -14.46 | 2.01 | -8.08 |
| | | | | | | | | | |
| Control 1 | -11.36 | -0.66 | -11.03 | -44.69 | -5.53 | -11.61 | 15.53 | 2.23 | -4.16 |
| Control 2 | -5.46 | 0.50 | 11.58 | 6.55 | 0.85 | -21.75 | 4.78 | 1.02 | 0.38 |
| Control 3 | -14.02 | 6.51 | -19.95 | -8.84 | -12.36 | 11.69 | -11.03 | 3.67 | -12.12 |
| Control 4 | -3.62 | 2.38 | -4.08 | 10.94 | 5.15 | 87.89 | -2.39 | 3.14 | -1.42 |
| Control 5 | -27.11 | 10.84 | -5.36 | -10.64 | -17.97 | 10.14 | 6.52 | 1.57 | -0.55 |

=Not significant difference (<10% for area and flow, <15% for velocity)

=Significant difference ((L<R)>10% for area and flow, (L>R)>15% for velocity)

= Significant difference in opposite direction ((L>R)>10% for area and flow, (L<R)>15% for velocity)

## Appendix 6 Graphs of external iliac artery in patients

| | Cross sectional area ($mm^2$) | Flow (l/min) | Maximum velocity (cm/s) |
|---|---|---|---|
| atient 1 | 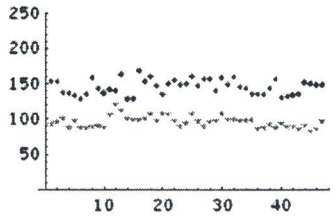 | 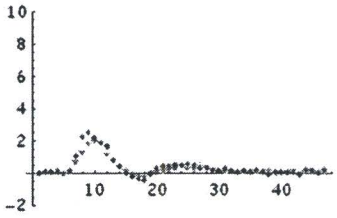 | 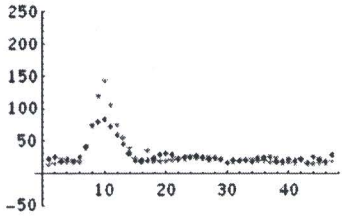 |
| atient 2 | 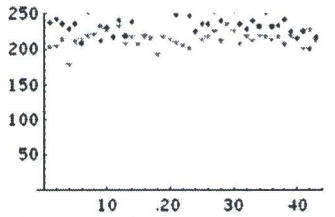 | 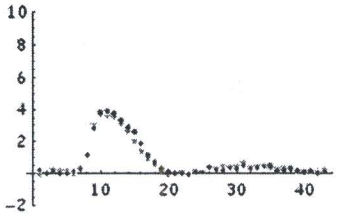 | 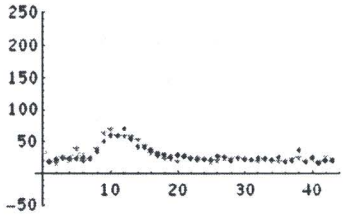 |
| atient 3 | 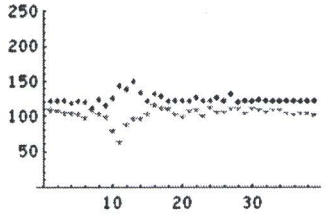 | 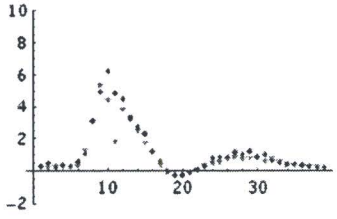 | 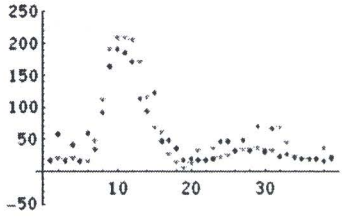 |
| atient 4 | 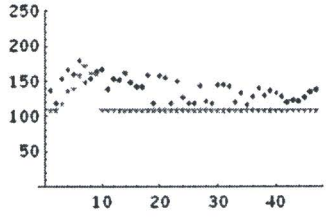 | 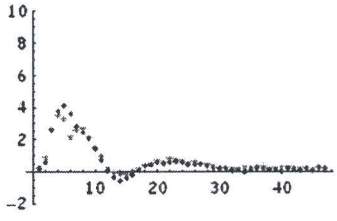 | 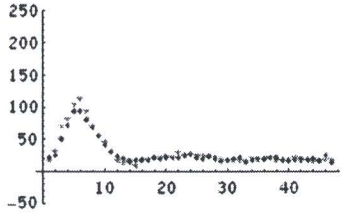 |
| atient 5 | 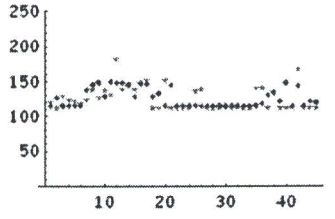 | 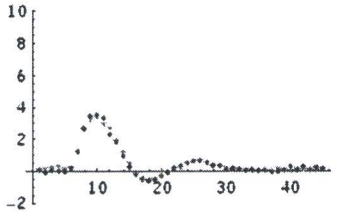 | 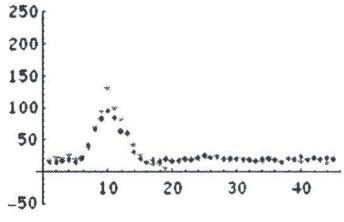 |
| atient 6 | 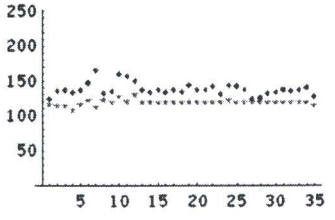 | 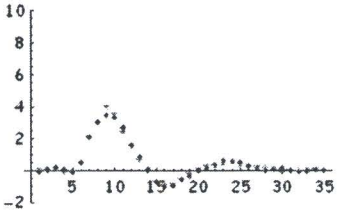 | 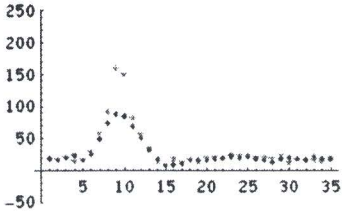 |

★ = Left external iliac artery, with intra vascular damage ◆ =right external iliac artery, healthy

Patient 7

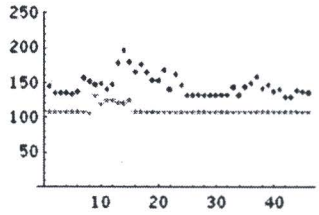


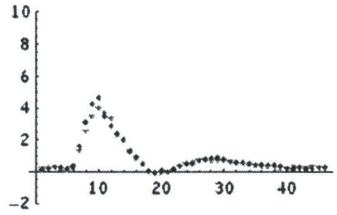


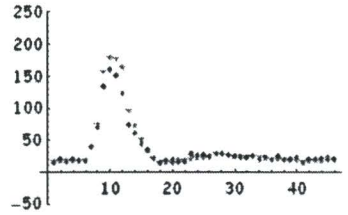


Patient 8 No quantitative flow images were made of the external iliac artery of patient 8

Patient 9